Molecular Microbiology

WILEY

RESEARCH ARTICLE OPEN ACCESS

Cytosolic Factors Controlling PASTA Kinase-Dependent ReoM Phosphorylation

Patricia Rothe[1] | Sabrina Wamp[1] | Lisa Rosemeyer[1] | Jeanine Rismondo[2] | Joerg Doellinger[3] | Angelika Gründling[2] | Sven Halbedel[1,4]

[1]FG11 Division of Enteropathogenic Bacteria and Legionella, Robert Koch Institute, Wernigerode, Germany | [2]Section of Molecular Microbiology and Centre for Bacterial Resistance Biology, Imperial College London, London, UK | [3]ZBS6 – Proteomics and Spectroscopy, Centre for Biological Threats and Special Pathogens, Robert Koch Institute, Berlin, Germany | [4]Institute for Medical Microbiology and Hospital Hygiene, Otto von Guericke University Magdeburg, Magdeburg, Germany

Correspondence: Sven Halbedel (halbedels@rki.de)

Received: 26 June 2024 | **Revised:** 11 August 2024 | **Accepted:** 14 August 2024

Funding: This work was supported by Deutsche Forschungsgemeinschaft, HA 6830/1-2, HA 6830/4-1.

Keywords: carboxyvinyltransferase | MurZ | protease adaptor | serine/threonine protein kinase | UDP-GlcNAc

ABSTRACT

Bacteria adapt the biosynthesis of their envelopes to specific growth conditions and prevailing stress factors. Peptidoglycan (PG) is the major component of the cell wall in Gram-positive bacteria, where PASTA kinases play a central role in PG biosynthesis regulation. Despite their importance for growth, cell division and antibiotic resistance, the mechanisms of PASTA kinase activation are not fully understood. ReoM, a recently discovered cytosolic phosphoprotein, is one of the main substrates of the PASTA kinase PrkA in the Gram-positive human pathogen *Listeria monocytogenes*. Depending on its phosphorylation, ReoM controls proteolytic stability of MurA, the first enzyme in the PG biosynthesis pathway. The late cell division protein GpsB has been implicated in PASTA kinase signalling. Consistently, we show that *L. monocytogenes prkA* and *gpsB* mutants phenocopied each other. Analysis of in vivo ReoM phosphorylation confirmed GpsB as an activator of PrkA leading to the description of structural features in GpsB that are important for kinase activation. We further show that ReoM phosphorylation is growth phase-dependent and that this kinetic is reliant on the protein phosphatase PrpC. ReoM phosphorylation was inhibited in mutants with defects in MurA degradation, leading to the discovery that MurA overexpression prevented ReoM phosphorylation. Overexpressed MurA must be able to bind its substrates and interact with ReoM to exert this effect, but the extracellular PASTA domains of PrkA or MurJ flippases were not required. Our results indicate that intracellular signals control ReoM phosphorylation and extend current models describing the mechanisms of PASTA kinase activation.

1 | Introduction

The main component of bacterial cell walls is peptidoglycan (PG), a network of glycan strands that are connected with each other by short peptide bridges. This mesh engulfs the cell and serves as a protective layer against external influences but also acts as a mechanical antagonist of cellular turgor. PG constitutes up to ~30% of the dry weight of a Gram-positive bacterial cell and therefore requires a high amount of precursor molecules and energy equivalents for its biosynthesis. Due to these massive energy costs, PG biosynthesis is closely coordinated with growth and nutrient supply and can also be activated in response to PG damage (Egan et al. 2017; Asai 2018; Helmann 2016). Biosynthesis of PG starts in the cytoplasm with the consumption of UDP-*N*-acetylglucosamine (UDP-GlcNAc) by the MurA and MurB enzymes that sequentially build up UDP-*N*-acetylmuramic acid (UDP-MurNAc). Further reactions assemble a pentapeptide side chain at the MurNAc

unit, transfer the resulting molecule onto the lipid carrier undecaprenyl phosphate and further add a second GlcNAc moiety (Barreteau et al. 2008; Teo and Roper 2015). The resulting lipid-linked pentapeptide-disaccharide (called lipid II) is then flipped across the membrane by so-called flippases (Meeske et al. 2015; Ruiz 2015). On the extracellular side, the disaccharide unit is transferred onto growing PG chains by glycosyltransferases and later crosslinked by transpeptidases. These latter two enzymatic activities are either provided by bifunctional class A penicillin-binding proteins (PBPs) or by SEDS-type glycosyltransferases that cooperate with class B PBPs that are mere transpeptidases (Sauvage et al. 2008; Meeske et al. 2016; Emami et al. 2017; Taguchi et al. 2019). The PG network is very dynamic and also remodelled by degradative enzymes to adjust size and shape for growth, division and development (Brogan and Rudner 2023). PG biosynthesis is fuelled either with UDP-GlcNAc generated by the GlmSMU enzymes from fructose-6-phosphate, an intermediate of glycolysis (Barreteau et al. 2008), or by salvage of PG precursors from environmental sources (Hottmann et al. 2021).

PG biosynthesis is controlled at multiple steps in the pathway and by different regulatory mechanisms. This includes transcriptional activation of biosynthetic and PG remodelling genes by alternative sigma factors and two-component systems (Helmann 2016; Timmler et al. 2022; Takada and Yoshikawa 2018), regulation of *glmS* translation through a metabolite-sensitive riboswitch (Winkler et al. 2004; Galinier et al. 2023), control of MurA protein stability (Kock, Gerth, and Hecker 2004; Wamp et al. 2020; Mascari, Little, and Kristich 2023), negative feedback inhibition of enzyme activities by downstream intermediates (Mizyed et al. 2005; Foulquier et al. 2020; Deng et al. 2006), activation of PBPs and their recruitment into protein complexes by interaction with scaffolding proteins (Rismondo et al. 2016; Cleverley et al. 2019; Egan, Errington, and Vollmer 2020) and enzyme phosphorylation by PASTA domain containing serine/threonine protein kinases (Kieser et al. 2015; Boutte et al. 2016; Gee et al. 2012).

We and others have described a central PASTA kinase-dependent mechanism of PG biosynthesis regulation (Figure 1). This mechanism controls the proteolytic degradation of MurA by the ClpCP protease (Wamp et al. 2020; Kelliher et al. 2021; Mascari, Little, and Kristich 2023; Tsui et al. 2023). MurA, which catalyses the first committed step in the PG biosynthesis pathway, is a known ClpCP substrate in *Bacillus subtilis*, *Listeria monocytogenes*, *Enterococcus faecalis* and *Staphylococcus aureus* (Kock, Gerth, and Hecker 2004; Wamp et al. 2020; Mascari, Little, and Kristich 2023; Graham, Lei, and Lee 2013). MurA degradation is highly regulated and requires the assistance of three additional proteins: ReoM (IreB in *E. faecalis*), ReoY and MurZ (also known as MurAB or MurA2) (Wamp et al. 2020; Kelliher et al. 2021; Mascari, Little, and Kristich 2023; Rismondo, Bender, and Halbedel 2017). One of these, ReoM, is phosphorylated at a conserved threonine residue (Thr-7 in *L. monocytogenes* ReoM) by its associated PASTA kinase, called PrkA in *L. monocytogenes* (Hall et al. 2013; Wamp et al. 2020; Kelliher et al. 2021). In the unphosphorylated form, ReoM directly interacts with MurA and hands it over to ClpCP for degradation (Wamp et al. 2020, 2022; Mascari, Little, and Kristich 2023). However, upon phosphorylation of ReoM at Thr-7 by PrkA, P~ReoM cannot bind MurA any longer,

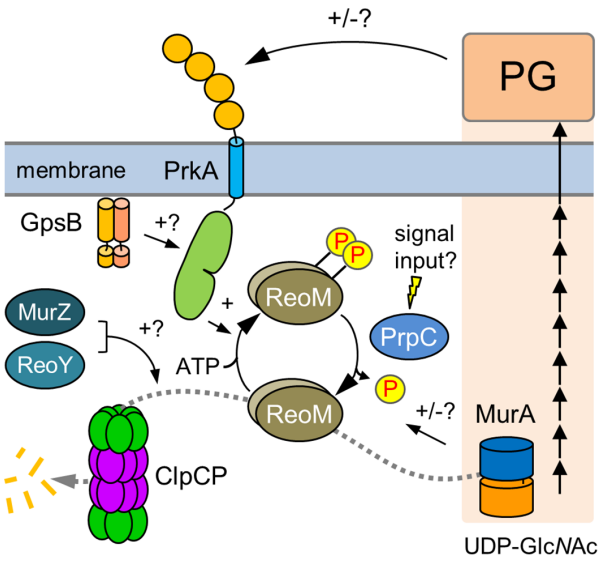

FIGURE 1 | Control of MurA degradation through PrkA-dependent phosphorylation of ReoM. Model describing the known regulators controlling phosphorylation of ReoM and MurA proteolytic stability. ReoM interacts with MurA to initiate ClpCP-dependent MurA degradation. MurA degradation by ClpCP is also dependent on ReoY and MurZ but for reasons that are not understood. MurA cannot bind ReoM anymore upon phosphorylation of ReoM by PrkA, which prevents MurA degradation and activates peptidoglycan (PG) biosynthesis. PrkA is activated by GpsB in several species by an unknown mechanism. Furthermore, PrkA is supposed to be controlled in an allosteric way by intermediates and end products of PG biosynthesis, but evidence supporting this theory is limited. PrpC reverses ReoM phosphorylation but it is unknown whether PrpC is constitutively active or subject to regulation. It was also not studied whether MurA has a regulatory role in this system.

which then accumulates (Wamp et al. 2020; Mascari, Little, and Kristich 2023; Sun, Hurlimann, and Garner 2023). The roles of ReoY and MurZ in this process are not well understood, but bacterial two hybrid data suggest that ReoY binds ClpCP as well as ReoM and therefore likely acts as a bridge between both (Wamp et al. 2020). MurZ is a paralogue of MurA but cannot take over its function in *B. subtilis* and *L. monocytogenes* (Rismondo, Bender, and Halbedel 2017; Kock, Gerth, and Hecker 2004), whereas the two MurA homologues of *E. faecalis*, *S. aureus* and *Streptococcus pneumoniae* can at least partially replace each other (Vesic and Kristich 2012; Blake et al. 2009; Du et al. 2000).

MurA enzymes consist of two globular domains and undergo conformational changes upon substrate binding. While the interdomain cleft is open in unliganded MurA, substrate binding induces a movement of the two domains towards each other so that liganded MurA adopts a more compact conformation (Schönbrunn et al. 1998). Substrate binding was required for IreB (the *E. faecalis* homologue of ReoM) to interact with MurAA from *E. faecalis* (Mascari, Little, and Kristich 2023), suggesting that ReoM only binds MurA in its closed conformation.

ReoM phosphorylation is reversed by the protein phosphatase PrpC (Wamp et al. 2020), however, neither the mechanisms controlling PrkA or PrpC activity are fully understood. PASTA kinases of *B. subtilis*, *E. faecalis* and *S. pneumoniae* are activated by GpsB, a late cell division protein with transient septal

localisation (Claessen et al. 2008; Fleurie et al. 2014; Pompeo et al. 2015; Minton et al. 2022). PASTA kinases have further been shown to bind lipid II and/or muropeptides through their extracellular PASTA domains (Mir et al. 2011; Hardt et al. 2017; Kaur et al. 2019). When PknB, the PASTA kinase of *Mycobacterium tuberculosis*, is modified in a way such that it can no longer bind lipid II, the protein becomes hyperactive (Kaur et al. 2019), suggesting an inhibitory role of lipid II.

Here, we investigated the regulation of ReoM phosphorylation in *L. monocytogenes*. For this, we established a method to directly measure ReoM phosphorylation in vivo using a ReoM-specific antibody and separation of differently phosphorylated ReoM species by native polyacrylamide gel electrophoresis.

2 | Results

2.1 | *L. monocytogenes* Mutants in *gpsB* and *prkA* Phenocopy Each Other

We previously demonstrated that an *L. monocytogenes* Δ*gpsB* mutant cannot grow at increased temperatures (Rismondo et al. 2016). However, this growth defect was suppressed by mutations in *clpC*, *reoY*, *reoM*, *murA*, *murZ* and *prpC* (Rismondo, Bender, and Halbedel 2017; Wamp et al. 2020, 2022). Interestingly, a similar spectrum of suppressor mutations was reported by Kelliher *et al*. to correct the hypersensitivity of a conditional *prkA* mutant against ceftriaxone (Kelliher et al. 2021) (Figure 2A). This overlap in the spectrum of suppressor mutations suggested that GpsB and PrkA could act in the same cellular pathway(s) and—as a consequence—that inactivation of their genes results in similar phenotypes. The *prkA* gene is essential in *L. monocytogenes* strain EGD-e (Wamp et al. 2020), but deletion of the C-terminal PASTA domains is tolerated and generates a partial *prkA* phenotype (Fischer et al. 2022). To test the assumed phenotypic similarity, we compared the ceftriaxone sensitivity of *gpsB* and *prkA* mutants. An *L. monocytogenes* mutant lacking the PrkA PASTA domains (*prkA*ΔC) was indeed more susceptible against ceftriaxone than wild type. Likewise, depletion of PrkA resulted in increased ceftriaxone susceptibility (when background growth of an i*prkA* strain on agar plates not containing IPTG was exploited for determination of the minimal inhibitory ceftriaxone concentration). The Δ*gpsB* mutant was also hypersensitive against ceftriaxone (Figure 2B), as was reported recently in another *L. monocytogenes* strain background (Kelliher, Daanen, and Sauer 2023). Furthermore, we also found that the *prkA*ΔC mutant showed a pronounced growth defect at 42°C (Figure 2C,D), as is known for the Δ*gpsB* mutant (Rismondo et al. 2016). Another characteristic phenotype of the Δ*gpsB* mutant emerges when the *divIVA* gene, required for division site selection and daughter cell separation (Halbedel et al. 2012; Kaval, Rismondo, and Halbedel 2014), is additionally deleted in the same strain: Δ*gpsB* Δ*divIVA* double mutant cells are considerably longer compared to either single mutant (Rismondo et al. 2016). Interestingly, a similar elongation of cells was observed in a *prkA*ΔC Δ*divIVA* double mutant (Figures 2E and S1). Moreover, the *prkA*ΔC mutant was less prone to lysis when treated with lysozyme compared to wild type. A similar phenotype had been reported for a Δ*gpsB* mutant (Rismondo et al. 2018) and was confirmed here (Figure 2F). Taken together, this shows that mutants in *prkA* and *gpsB* generally exhibit similar phenotypes, reinforcing the idea that PrkA and GpsB cooperate.

2.2 | In Vivo PrkA Activity Depends on GpsB

Given the phenotypic similarities of *gpsB* and *prkA* mutants described above, it was reasonable to assume that *L. monocytogenes* PrkA requires GpsB for activity, as demonstrated for other Gr-positive bacteria (Fleurie et al. 2014; Pompeo et al. 2015; Minton et al. 2022). Previously, it has been reported that P~ReoM can be separated from unphosphorylated ReoM using native PAGE in in vitro experiments (Wamp et al. 2020). To use this technique for separation of the two ReoM species in cellular extracts, an antiserum was generated against *L. monocytogenes* ReoM. During initial experiments, this antiserum did only poorly detect ReoM in wild-type extracts. We thus introduced a *reoM-his* allele under control of the strong P_{help} promoter to facilitate ReoM detection (Monk, Gahan, and Hill 2008). This allowed the detection of a single ReoM-His species in the wild type (Figure 3A). For comparison with cells lacking PrkA, we inserted the *reoM-his* allele into the Δ*prkA murA N197D* background, where lethality of the Δ*prkA* deletion is overcome by the *murA N197D* mutation, which renders MurA resistant to ClpCP-dependent degradation as it prevents ReoM binding to MurA (Wamp et al. 2022). ReoM-His migrated slower in this strain (Figure 3A), which is in good agreement with the retarded migration of unphosphorylated ReoM observed in vitro (Wamp et al. 2020). In contrast to the wild type, two ReoM species were detected in the *murA N197D* background, one at the same height as in wild type and an additional one, the origin of which is currently unclear, but probably corresponds to a ReoM/ReoM-P heterodimer (Figure 3A). Next, we tried to introduce the *reoM-his* allele into the Δ*gpsB* mutant, but consistent with the idea that GpsB is required for PrkA activity and with the toxicity of unphosphorylated ReoM, this was never possible. Therefore, *reoM-his* was brought into the Δ*gpsB murAN197D* background, yielding a viable strain. ReoM-His migrated at the position of the unphosphorylated ReoM species observed in the Δ*prkA murAN197D* strain (Figure 3A), supporting the idea that GpsB is required for PrkA activity in *L. monocytogenes*.

We then purified the two ReoM-His species from the two *L. monocytogenes* strains LMJD22 (*prkA*$^+$) and LMPR5 (Δ*prkA murA N197D*) (Figure 3B). ReoM-His purified from the *prkA*$^+$ strain ran faster through the native gel than ReoM-His purified from the Δ*prkA murA N197D* strain, the position of which was similar to unphosphorylated ReoM-Strep purified from *E. coli* (Figure 3B). The two ReoM-His species were subjected to mass spectrometry, which showed phosphorylation at Thr-7 and Tyr-10 in ReoM purified from wild-type background (LMJD22), while ReoM purified from Δ*prkA* cells (LMPR5) was only phosphorylated at Tyr-10.

As final proof that we look at ReoM phosphorylated at Thr-7 here, we analysed the in vivo ReoM phosphorylation patterns in a strain expressing a phospho-ablative *reoM T7A-his* variant as a second *reoM* copy (LMPR42). As expected, ReoM T7A-His migrated at the position of the unphosphorylated ReoM in this strain (Figure 3C), however, a faint signal at the position of the phosphorylated protein remained, which corresponded to the native endogenous ReoM, as this signal was no longer detected upon *reoM* deletion (strain LMPR48, Figure 3C).

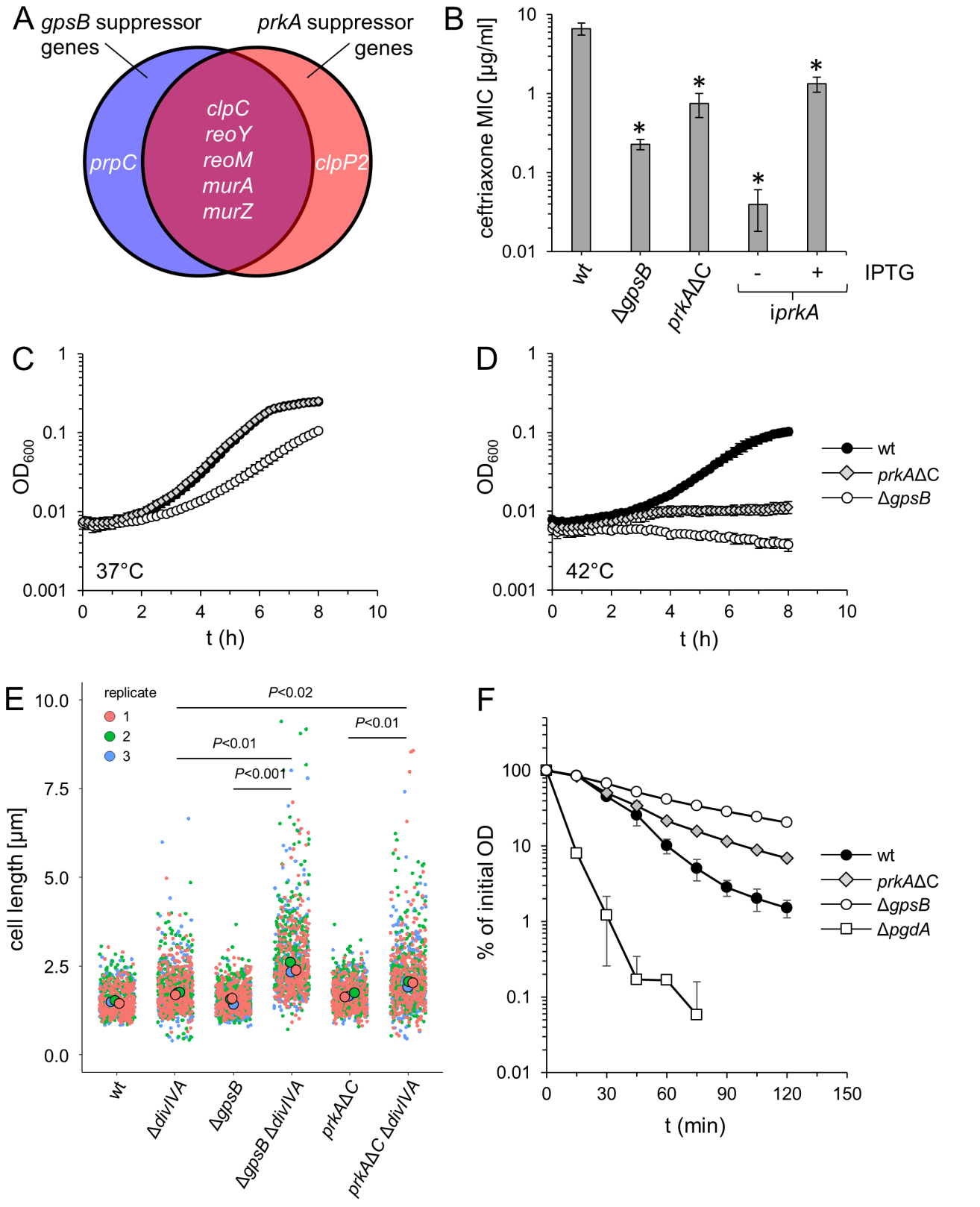

FIGURE 2 | Legend on next page.

2.3 | ReoM Phosphorylation Is Generally Insensitive to Defects in Cell Division

GpsB is a late cell division protein (Halbedel and Lewis 2019) and PASTA kinases are known to localise to cell division sites in *B. subtilis* and *S. pneumoniae* (Beilharz et al. 2012; Pompeo et al. 2018). We therefore wondered, whether cell division proteins other than GpsB also influence PrkA activity and analysed phosphorylation of endogenous ReoM, which became detectable by loading larger amounts of protein, in strains lacking the non-essential cell division genes *divIVA*, *pbpA1*, *sepF*, *zapA*, *minCD* and *minJ*. However, ReoM was found to be

FIGURE 2 | Phenotypic similarity of *L. monocytogenes gpsB* and *prkA* mutants. (A) Mutants in *gpsB* and *prkA* are suppressed by mutations in the same set of genes. Venn diagram showing genes that acquired mutations in suppressors of an *L. monocytogenes* Δ*gpsB* mutant (EGD-e background) (Rismondo, Bender, and Halbedel 2017; Wamp et al. 2020, 2022) and in suppressors of a conditional *prkA* mutant (10403S background) (Kelliher et al. 2021). (B) Mutants in *gpsB* and *prkA* are hypersensitive to ceftriaxone. Minimal inhibitory concentrations of ceftriaxone for *L. monocytogenes* strains EGD-e (wt), LMJR19 (Δ*gpsB*), LMS278 (*prkA*ΔC) and LMSW84 (i*prkA*) grown ± IPTG. The experiment was repeated three times and average values and standard deviations are shown. Asterisks indicate statistically significant differences compared to wild type ($p < 0.01$, *t*-test with Bonferroni-Holm correction). (C, D) *gpsB* and *prkA* mutants cannot grow at 42°C. Growth of *L. monocytogenes* strains EGD-e (wt), LMJR19 (Δ*gpsB*) and LMS278 (*prkA*ΔC) in BHI broth at 37°C (C) and 42°C (D). (E) Introduction of the Δ*divIVA* deletion into *gpsB* and *prkA* mutant strains results in strong cell elongation. Superblots showing cell lengths of *L. monocytogenes* strains EGD-e (wt), LMS2 (Δ*divIVA*), LMJR19 (Δ*gpsB*), LMJR28 (Δ*gpsB* Δ*divIVA*), LMS278 (*prkA*ΔC) and LMPR27 (*prkA*ΔC Δ*divIVA*) during mid-logarithmic growth in BHI broth at 37°C. Three hundred cells per strain were measured per replicate. Median values for each replicate are shown and significance levels (*t*-test with Bonferroni-Holm correction) are indicated. (F) Mutants in *gpsB* and *prkA* are less susceptible to lysozyme. *L. monocytogenes* strains EGD-e (wt), LMJR19 (Δ*gpsB*), LMS278 (*prkA*ΔC) and LMS163 (Δ*pgdA*) were challenged with lysozyme and the decline of optical density over time was recorded. Average values and standard deviations from three technical replicates are shown. The lysozyme-sensitive Δ*pgdA* mutant was included for comparison.

phosphorylated in all these mutants except the Δ*gpsB* strain (Figure S2A), demonstrating that the effect of GpsB on PrkA was specific.

Next, we asked whether distortion of cell division by depletion of an essential cell division protein would influence ReoM phosphorylation. PBP B2 is required for septal PG biosynthesis and its depletion blocks cell division leading to the formation of long non-septated filaments (Rismondo et al. 2015). We depleted PBP B2 in strain LMJR18 and analysed the phosphorylation of endogenous ReoM by Western blotting. However, no effects on ReoM phosphorylation were found (Figure S2B). Likewise, depletion of PBP B1 (strain LMJR27), necessary for PG biosynthesis along the lateral cell cylinder and maintenance of rod shape (Rismondo et al. 2015), did not interfere with phosphorylation of endogenous ReoM (Figure S2B). Apparently, ReoM phosphorylation is not disturbed by defects in cell division in general and also does not depend on the two specific modes of PG biosynthesis at the septum and the lateral wall.

2.4 | ReoM Phosphorylation Requires Hexameric GpsB

GpsB is a hexameric membrane-binding protein known to interact with PBP A1 through a defined cleft in its surface (Rismondo et al. 2016; Cleverley et al. 2016, 2019). Moreover, GpsB itself is phosphorylated by PrkA at various threonine residues including Thr-88 (Kelliher et al. 2021; Cleverley et al. 2016; Pompeo et al. 2015). To address the question which functionalities in GpsB support its role in PrkA activation, we determined the ReoM phosphorylation pattern in strains expressing *gpsB* alleles with specific functional mutations. As can be seen in Figure 4, wild-type-like ReoM phosphorylation patterns were observed in *gpsB* L24A and R24A mutants. These mutations interfere with the binding of GpsB to the cytoplasmic membrane (Rismondo et al. 2016). Likewise, normal ReoM phosphorylation was detected in strains carrying *gpsB* alleles with mutations preventing PBP A1 binding (Y27A-I40A) (Cleverley et al. 2019) (Figure 4). Remarkably, normal ReoM phosphorylation was also observed in a strain, in which *gpsB* carried the phospho-ablative T88A mutation. When the same residue was mutated in a phosphomimetic manner (T88D), a slight reduction in ReoM phosphorylation became apparent (Figure 4). In contrast, strong effects on ReoM phosphorylation were observed in *gpsB* mutants, in which mutations prevented the interaction of the two trimeric C-terminal domains required for hexamer formation (F91A, L94A and F105A) (Cleverley et al. 2016) or when even the trimers could not be formed due to mutations in residues essential for formation of the trimer stabilising salt bridges (R96A and E101A) (Rismondo et al. 2016) (Figure 4). Importantly, previous work showed that all *gpsB* mutant alleles analysed here were expressed to wild-type-like levels (Rismondo et al. 2016; Cleverley et al. 2016). This shows that the formation of the hexameric GpsB complex is of great importance for PrkA activation, while GpsB does not need to be membrane-bound or bound to PBP A1 to exert this effect. Likewise, phosphorylation of GpsB at Thr-88 seems to play only a minor role in activation of PrkA compared to the structural effects.

2.5 | ReoM Phosphorylation Changes With Growth Progression

Next, ReoM phosphorylation was studied during different stages of growth. For this, a culture of strain EGD-e was grown in BHI broth at 37°C and samples were taken at different optical densities. ReoM was found to be phosphorylated during the exponential growth phase but a shift towards unphosphorylated ReoM was detected during the stationary phase (Figure 5A). We also observed that MurA levels declined during growth and were reduced to 13 ± 6% at the late stationary phase ($OD_{600} = 3.0$) compared to the original level detected at an OD_{600} of 0.5 (Figure 5A). This demonstrates that ReoM phosphorylation and MurA levels decline at the stationary phase.

2.6 | Control of ReoM Phosphorylation by PrkA and PrpC

The antagonist of PrkA is the phosphatase PrpC, which dephosphorylates P~ReoM in vitro (Wamp et al. 2020). The *prpC* gene is essential in wild type (Wamp et al. 2020; Fischer et al. 2022). To test for PrpC phosphatase activity in vivo despite this limitation, we analysed ReoM phosphorylation in a Δ*gpsB* Δ*prpC* mutant background, where deletion of *prpC* is tolerated (Wamp et al. 2022). ReoM was fully phosphorylated in this strain background, even though no P~ReoM was found in the parental Δ*gpsB* mutant that still contained *prpC* (Figure S3A). Thus, PrpC dephosphorylates

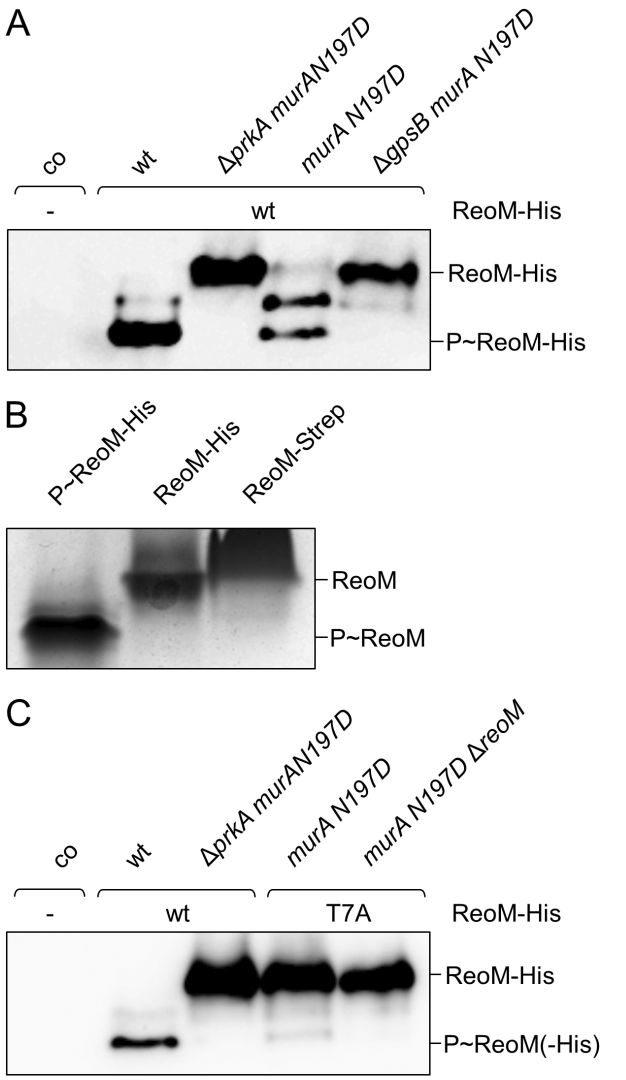

FIGURE 3 | GpsB is required for *L. monocytogenes* PrkA activity. (A) Western blot after native PAGE for detection and separation of the different forms of ReoM-His in *L. monocytogenes* strains LMJD22 (labelled 'wt'), LMPR5 ('Δ*prkA murA N197D*'), LMPR9 ('*murA N197D*') and LMPR10 ('Δ*gpsB murA N197D*'). *L. monocytogenes* EGD-e ('co') was included as a negative control. The presence of ectopically expressed ReoM-His in the analysed strains is specified. (B) Native PAGE loaded with ReoM-His~P purified from strain LMJD22 (*prkA*$^+$) and with unphosphorylated ReoM-His, which was purified from the Δ*prkA murA N197D* strain LMPR5. ReoM-Strep directly purified from *E. coli* was included as a control. (C) In vivo ReoM phosphorylation requires Thr-7. Western blot after native PAGE for ReoM detection in *L. monocytogenes* strains EGD-e (labelled 'co'), LMJD22 ('wt'), LMPR5 ('Δ*prkA murA N197D*'), LMPR42 ('*murA N197D*') and LMPR48 ('*murA N197D* Δ*reoM*'). The presence of ectopically expressed ReoM-His and T7A variants is specified.

ReoM in vivo, which in turn implies that PrkA must still have residual kinase activity despite the absence of GpsB.

We next addressed the contribution of PrpC to the observed growth phase-dependent ReoM phosphorylation pattern and determined ReoM phosphorylation in the i*prpC* strain LMSW83 allowing IPTG-dependent PrpC production. When this strain was grown without IPTG, the decline in ReoM phosphorylation and reduction of MurA levels during late stages of growth was delayed (Figure 5B), indicating that PrpC contributes to the growth phase-dependent ReoM dephosphorylation, particularly during the stationary phase.

Similar to *prpC*, the *prkA* gene is essential in EGD-e, but deletion of the PASTA domains was tolerated (Fischer et al. 2022). We therefore wondered how deletion of the PASTA domains would affect ReoM phosphorylation. The ReoM migration pattern shifted from the fully phosphorylated to the monophosphorylated dimer and the unphosphorylated forms in a *prkA*ΔC mutant lacking all PASTA domains (Figure S3B). Thus, the PASTA domains are required for full PrkA activity. Next, we investigated whether the intermediate kinase activity observed in the *prkA*ΔC background was still GpsB-dependent and compared ReoM phosphorylation in the *prkA*ΔC *murA N197D* and the Δ*gpsB prkA*ΔC *murA N197D* mutants. Deletion of *gpsB* was dominant over the *prkA*ΔC mutation, as only unphosphorylated ReoM-His was detected in the Δ*gpsB prkA*ΔC *murA N197D* mutant (Figure S3C). This shows that GpsB exerts its impact on PrkA in a manner that is independent of the PASTA domains.

2.7 | ReoM Phosphorylation Responds to MurA Accumulation

ReoM acts in concert with ReoY and MurZ to control MurA degradation via ClpCP (Wamp et al. 2020, 2022). We wondered whether any of these proteins would be involved in the control of P~ReoM formation and analysed the phosphorylation of endogenous ReoM in Δ*clpC*, Δ*murZ* and Δ*reoY* mutants. Remarkably, most ReoM was found unphosphorylated in each of these mutants (Figure 6A). In contrast, total ReoM levels were not altered after separation of the same samples using SDS PAGE gels (Figure 6A). MurA strongly accumulates in mutants lacking *clpC*, *murZ* or *reoY* (Rismondo, Bender, and Halbedel 2017; Wamp et al. 2020) (Figure 6A), but due to the pleiotropic effect that can be expected upon disrupting ClpCP-dependent proteolysis, it is not known whether MurA accumulation is the underlying reason for the effect on ReoM phosphorylation. To address this, we tested the effect of *murA* overexpression on ReoM phosphorylation in strain LMJR123, carrying an IPTG-inducible copy of *murA*. The addition of IPTG led to a strong accumulation of MurA and to a concomitant reduction of ReoM phosphorylation in this strain (Figure 6B). In contrast to this, ReoM phosphorylation was not affected by overexpression of MurZ (Figure S4). Furthermore, we observed that depletion of MurA from Δ*clpC* cells partially restored the phosphorylation of ReoM (Figure 6B). This demonstrates that ReoM phosphorylation is sensitive to the level of MurA.

Work in *M. tuberculosis* suggested that PASTA kinases can be inhibited by lipid II through interaction with their extracellular PASTA domains (Kaur et al. 2019). Inspired by this result, we assumed that MurA accumulation would lead to higher lipid II levels that in turn could interfere with ReoM phosphorylation by inhibition of PrkA through interaction with its PASTA domains. To test this, we first wanted to determine ReoM phosphorylation in a Δ*clpC* mutant lacking the two MurJ-like lipid II flippases to prevent lipid II transport to the extracellular site. As simultaneous deletion of both *murJ* genes was not possible, a strain was

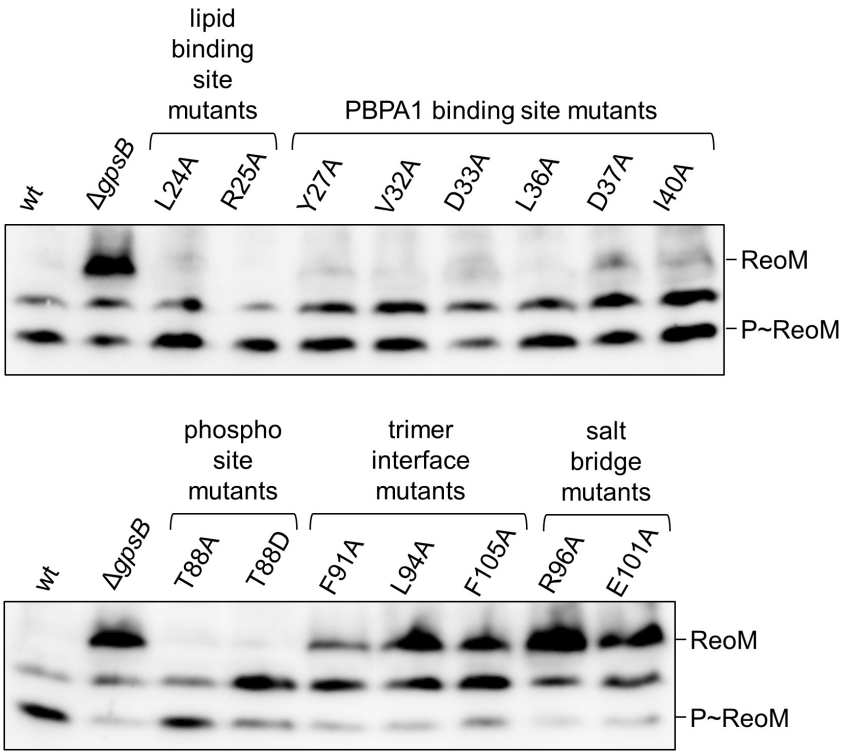

FIGURE 4 | Effect of functional *gpsB* mutations on PrkA activity. Western blots after native PAGE for analysis of in vivo ReoM phosphorylation in *L. monocytogenes* strains expressing selected *gpsB* mutant alleles with different effects on GpsB function. *L. monocytogenes* strains were EGD-e (wt), LMJR19 (Δ*gpsB*), LMJR68 (L24A), LMJR4 (R25A), LMJR130 (Y27A), LMJR131 (V32A), LMJR135 (D33A), LMJR132 (L36A), LMJR133 (D37A), LMJR134 (I40A), LMJR161 (T88A), LMJR162 (T88D), LMS185 (F91A), LMS186 (L94A), LMS187 (F105A), LMJR163 (R96A) and LMJR164 (E101A). Strains were grown in BHI broth containing 1 mM IPTG at 37°C to mid-logarithmic growth before samples were taken.

generated in which an IPTG-dependent copy of *murJ2* (*lmo1625*, *LMRG_01341*) was expressed from an ectopic site and the *murJ2* and *murJ1* (*lmo1624*, *LMRG_01342*) genes were deleted from the chromosome. This strain showed a slight but significant growth retardation (Figure S5A) and a four-fold reduced resistance to lysozyme in the absence of IPTG (Figure S5B) indicating at least partial depletion of flippase activity. However, depletion of MurJ activity had no effect on ReoM phosphorylation (Figure 6C). Moreover, when MurJ activity was depleted in Δ*clpC* cells, ReoM phosphorylation was not restored (Figure 6C) as observed with depletion of MurA (Figure 6B). Apparently, prevention of lipid II transport across the cytoplasmic membrane does not interfere with ReoM phosphorylation. To test this idea further, the effect of MurA overexpression on ReoM phosphorylation was determined in *prkA*ΔC cells lacking the PrkA PASTA domains. In these cells, MurA overexpression still exerted a negative effect on ReoM phosphorylation despite the absence of the PASTA domains (Figure 6D). Thus, the PASTA domains of the *L. monocytogenes* PrkA protein do not seem to play a role in sensing the MurA level.

2.8 | Effect of Mutated MurA Variants on ReoM Phosphorylation

As our results contradict the concept of a negative feedback loop and the idea that accumulation of lipid II inhibits PrkA activity, we considered MurA as a direct effector of ReoM phosphorylation. We reasoned that MurA would lose the ability to interfere with ReoM phosphorylation if it is unable to bind ReoM. Therefore, we tested the effect of overproducing the MurA N197D and MurA S262L variants on ReoM phosphorylation, as both substitutions prevent the interaction of MurA with ReoM (Wamp et al. 2022). Remarkably, overproduction of neither of these two MurA variants prevented the phosphorylation of ReoM (Figure 7A), suggesting that a direct interaction between MurA and ReoM is needed.

MurA undergoes substantial conformational changes during substrate binding and catalysis. Unliganded apo-MurA is found in an open conformation, in which the flexible activation loop containing the catalytically important cysteine (C117 in *L. monocytogenes* MurA) is moved away from the enzyme. Upon substrate binding, the activation loop closes the UDP-GlcNAc binding site to bring phosphoenolpyruvate (PEP) into the vicinity of UDP-GlcNAc (i.e., closed conformation) (Schönbrunn et al. 1998; Skarzynski et al. 1996; Gautam, Rishi, and Tewari 2011; Zhu et al. 2012). Remarkably, *E. faecalis* IreB interacts with MurAA only, when MurAA is complexed with UDP-GlcNAc and fosfomycin (Mascari, Little, and Kristich 2023), a condition under which *E. coli* MurA adopts the closed conformation (Skarzynski et al. 1996).

We tested the effect of inactivating MurA substitutions either preventing UDP-GlcNAc binding (N23A) (Samland et al. 2001) or covalent PEP binding (K22V, C117A) (Kim et al. 1996; Samland, Amrhein, and Macheroux 1999) on ReoM phosphorylation. This showed that all mutated proteins were unable to suppress phosphorylation of ReoM (Figure 7B). The N23A

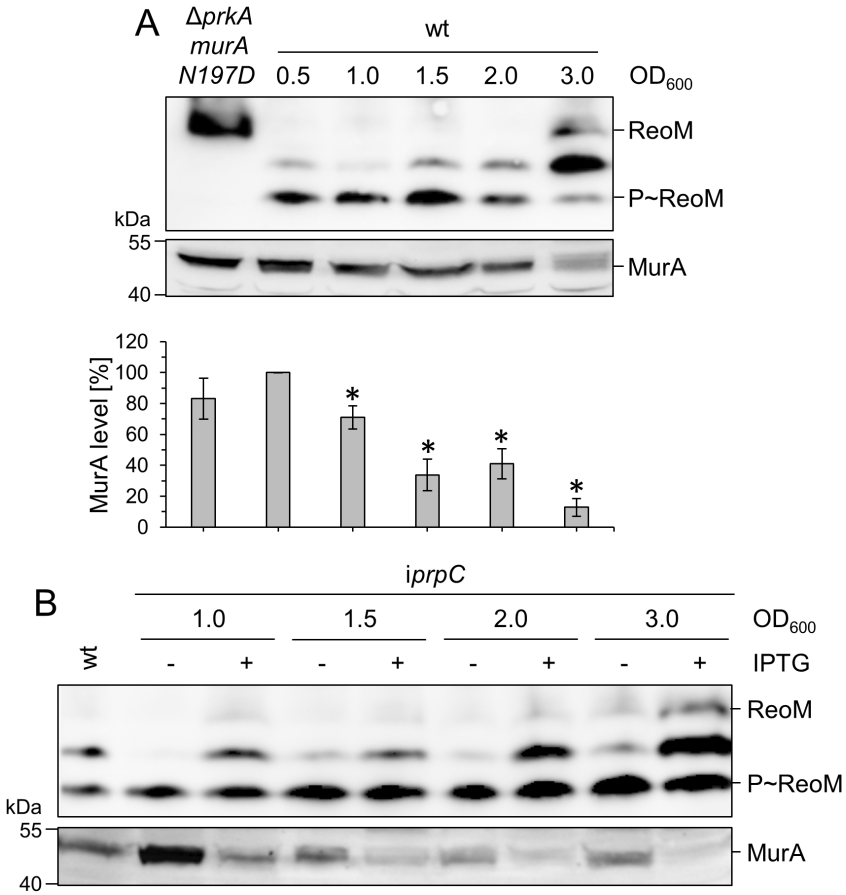

FIGURE 5 | Effect of growth phase on ReoM phosphorylation. (A) Growth phase-dependent ReoM phosphorylation and MurA levels. Western blot after native PAGE showing ReoM phosphorylation in *L. monocytogenes* strain EGD-e (wt) that was grown in BHI broth at 37°C to the indicated optical densities (upper panel). Strain LMS266 (Δ*prkA murA N197D*) was included as a negative control. Western blot after standard SDS PAGE to determine MurA levels in the same samples (middle panel). MurA signals were determined by densitometry and expressed as values relative to wild type at $OD_{600} = 0.5$ (bottom panel). Average values and standard deviations are shown ($n = 3$) and asterisks label statistically significant differences relative to wild type at $OD_{600} = 0.5$ ($p < 0.05$, *t*-test with Bonferroni-Holm correction). (B) Decline of ReoM phosphorylation and MurA levels in stationary phase depend on PrpC. Western blot after native PAGE showing ReoM phosphorylation in *L. monocytogenes* strains EGD-e (wt) and LMSW83 (i*prpC*) grown in BHI broth ±1 mM IPTG at 37°C to the indicated optical densities (upper panel). Western blot showing MurA levels in the same samples (lower panel).

protein is possibly locked in the open conformation because it cannot bind UDP-GlcNAc (Samland et al. 2001). The K22V mutant is also catalytically inactive; it cannot bind PEP covalently but it is not impaired in UDP-GlcNAc binding (Samland, Amrhein, and Macheroux 1999). The catalytic cysteine mutant still binds UDP-GlcNAc and can adopt a closed conformation (Skarzynski et al. 1998; Schönbrunn et al. 2000). However, covalent PEP binding is reduced and the protein cannot proceed through catalysis (Wanke and Amrhein 1993; Skarzynski et al. 1998; Zhu et al. 2012). This allows the conclusion that there is no MurA-dependent negative feedback on ReoM phosphorylation when MurA substrate binding is impaired.

2.9 | The MurA:ReoM Interaction Is Sensitive to ReoM Phosphorylation

According to our current model, ReoM phosphorylation regulates the interaction of ReoM with MurA. In this model, only unphosphorylated ReoM can form a complex with MurA and phosphorylation of ReoM prevents this (Wamp et al. 2020, 2022). However, this model has mostly been deduced from genetic data and direct evidence for the *L. monocytogenes* proteins is still missing. To test whether the interaction of MurA with ReoM depends on ReoM phosphorylation, we made use of the observation that MurA can be copurified from total cellular extracts with ReoM-His as the bait (Wamp et al. 2022). The essentiality of *prkA* is lost in the absence of *murZ* (Wamp et al. 2022). We therefore generated an isogenic pair of Δ*murZ* strains both expressing *reoM-his* and containing *prkA* (LMPR25) or not (LMPR29). As anticipated, MurA levels in these strains exceeded that of wild type approximately 9-10-fold due to impaired MurA degradation (Figure 8A, upper and lower panel), regardless of whether ReoM was phosphorylated or unphosphorylated (Figure 8A, middle panel). MurA copurified with ReoM-His from lysates of the *prkA*$^+$ strain (Figure 8B, upper panel) where most of it was phosphorylated (Figure 8A, middle panel). However, the amount of MurA that copurified with ReoM-His from lysates of the Δ*prkA* strain, where ReoM is not phosphorylated, was 3 ± 1-fold higher ($n = 3$, $p < 0.05$) although less ReoM-His material (0.7 ± 0.1-fold) was pulled down. This is in agreement with the idea that the MurA:ReoM interaction is prevented by phosphorylation of ReoM.

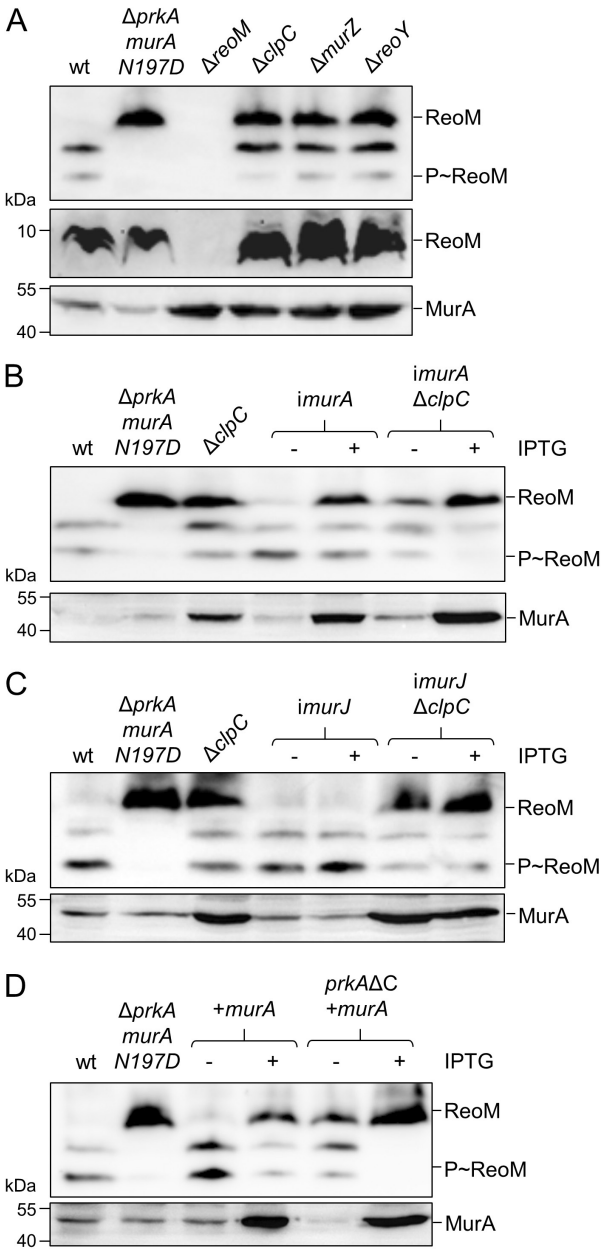

FIGURE 6 | Direct control of ReoM phosphorylation through the level of MurA. (A) ReoM phosphorylation requires ClpC, MurZ and ReoY. Phosphorylation of ReoM was analysed in strains EGD-e (wt), LMS266 (Δ*prkA murA N197D*), LMJR138 (Δ*clpC*), LMJR104 (Δ*murZ*) and LMSW32 (Δ*reoY*) (upper panel, separation by native PAGE). Absolute ReoM and MurA levels in the same set of strains were visualised in parallel Western blots using SDS PAGE gels for separation (ReoM: Middle panel, MurA: Lower panel). (B) MurA levels control ReoM phosphorylation in wild-type and Δ*clpC* cells. Western blots showing ReoM phosphorylation (upper blot) and MurA levels (bottom blot) in strains EGD-e (wt), LMS266 (Δ*prkA murA N197D*), LMJR138 (Δ*clpC*), LMJR123 (i*murA*) and LMPR52 (i*murA* Δ*clpC*) grown in BHI broth ±1 mM IPTG. (C) Control of ReoM phosphorylation through MurA is MurJ-independent. Western blots showing ReoM phosphorylation (upper blot) and MurA levels (bottom blot) in strains EGD-e (wt), LMS266 (Δ*prkA murA N197D*), LMJR138 (Δ*clpC*), ANG5140 (i*murJ*) and LMPR54 (i*murJ* Δ*clpC*) grown in BHI broth ±1 mM IPTG. (D) The MurA effect on ReoM phosphorylation does not involve the PASTA domains of PrkA. Western blots showing ReoM phosphorylation (upper blot) and MurA levels (bottom blot) in strains EGD-e (wt), LMS266 (Δ*prkA murA N197D*), LMJR116 (+*murA*) and LMPR49 (*prkA*ΔC + *murA*) grown in BHI broth ±1 mM IPTG.

Lastly, we tested whether ReoM would affect MurA activity. This idea was brought forward by Tsui and coworkers, who suggested that unphosphorylated *S. pneumoniae* ReoM could inhibit the activity of the MurA enzymes (Tsui et al. 2023). However, in vitro activity of *L. monocytogenes* MurA was not affected by the addition of unphosphorylated ReoM (Figure S6). Thus, the main role of *L. monocytogenes* ReoM is the regulation of MurA degradation by ClpCP.

3 | Discussion

3.1 | PASTA Kinase Activation by GpsB

We demonstrate that *L. monocytogenes* PrkA requires GpsB for full activity towards ReoM. This role of GpsB is specific as none of the other tested cell division proteins contributed to kinase activation and even in non-dividing PBP B1-depleted cells, normal ReoM phosphorylation was observed. Thus, PrkA activity is not dependent on cell division in *L. monocytogenes*, even though septal localisation of PASTA kinases in other species suggested such a link (Pompeo et al. 2018; Hardt et al. 2017; Zucchini et al. 2018; Mir et al. 2011). Given the phenotypic similarity of *L. monocytogenes gpsB* and *prkA* mutants and suppression of their phenotypes by an almost identical set of mutations (Rismondo, Bender, and Halbedel 2017; Wamp et al. 2020; Kelliher et al. 2021), the effect of GpsB on PrkA activity was expected. In good agreement, GpsB supported the activity of the *B. subtilis* PrkC kinase in vitro and was required for *E. faecalis* IreK activity in vivo (Pompeo et al. 2015; Minton et al. 2022; VanZeeland et al. 2023). GpsB belongs to the DivIVA/GpsB family of coiled-coil membrane-binding proteins that consist of N-terminal lipid binding domains fused to C-terminal multimerisation domains (Halbedel and Lewis 2019). These proteins recruit interacting proteins to curved membrane areas, to which they bind themselves, and partner recruitment can occur either through their N- or C-terminal domain (van Baarle et al. 2013; Halbedel and Lewis 2019). Highly conserved regions in the N-terminal domain of GpsB contribute to membrane and PBP A1 binding and mutations in these regions usually inactivate GpsB (Rismondo et al. 2016; Cleverley et al. 2019). We here show that GpsB did not need to bind membranes or PBP A1 for PrkA activation. However, mutations that abolished the tertiary structure of the hexameric GpsB C-terminus impaired activation of PrkA. Several possibilities appear plausible to explain this: (i) The interaction of GpsB with PrkA could be polyvalent and low affinity binding sites present in the N-terminal domains of GpsB monomers or dimers, which are known to interact with many other proteins (Cleverley et al. 2019; Halbedel and Lewis 2019; Sacco et al. 2024; Bartlett et al. 2024), form a high-affinity binding site in the GpsB hexamer, (ii) GpsB hexamers could be required for dimerisation of PrkA, which is discussed as a prerequisite for kinase activation (Barthe et al. 2010; Labbe and Kristich 2017), for PrkA multimerisation or for recruiting PrkA into complexes with other interaction partners, or (iii) the C-terminus of GpsB

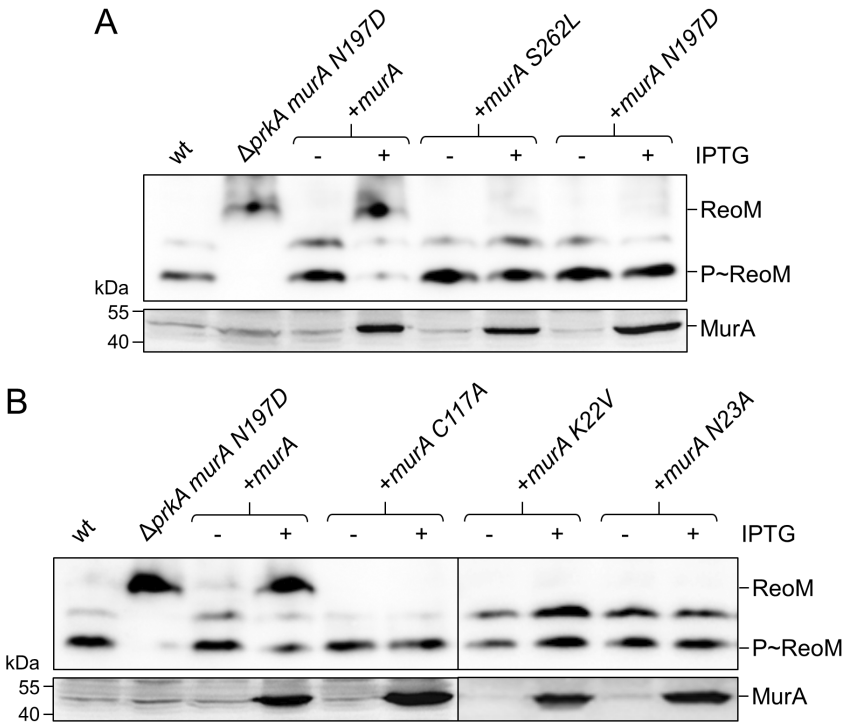

FIGURE 7 | Effect of functional *murA* mutations on ReoM phosphorylation. (A) MurA must interact with ReoM to control its phosphorylation. Western blots showing ReoM phosphorylation (upper blot) and MurA levels (bottom blot) in strains EGD-e (wt), LMS266 (Δ*prkA murA N197D*), LMJR116 (+*murA*), LMSW136 (+*murA S262L*) and LMSW137 (+*murA N197D*) grown in BHI broth ±1 mM IPTG. (B) The active site cysteine and residues important for substrate binding in MurA are essential for control of ReoM phosphorylation by MurA. Western blots showing ReoM phosphorylation (upper blot) and MurA levels (bottom blot) in strains EGD-e (wt), LMS266 (Δ*prkA murA N197D*), LMJR116 (+*murA*), LMPR51 (+*murA C117A*), LMPR57 (+*murA K22V*) and LMPR56 (+*murA N23A*) grown in BHI broth ±1 mM IPTG.

interacts with PrkA and needs to be hexameric for this. If so, then PrkA would be the first GpsB-binding protein described that interacts with the C-terminal domain of GpsB.

3.2 | Control of PrkA Activity During Growth

Control of PASTA kinase activity during cell growth and division is still an unsolved mystery. PASTA kinases are activated by muropeptides and/or lipid II binding to their PASTA domains (Mir et al. 2011; Hardt et al. 2017; Kaur et al. 2019). This idea is based on the observation that the PASTA kinases of *S. aureus* and *M. tuberculosis* interact with lipid II in vitro and lose this ability when their PASTA domains are deleted or mutated (Hardt et al. 2017; Kaur et al. 2019). Furthermore, dimerisation and septal localisation of PASTA kinases are also lost upon deletion of their PASTA domains (Pompeo et al. 2018; Rakette et al. 2012; Pallova et al. 2007; Hardt et al. 2017; Zucchini et al. 2018). PASTA domains are not required for kinase activity in general (Pompeo et al. 2018; Wamp et al. 2020; Rakette et al. 2012; Zucchini et al. 2018), but they are needed for full kinase activity (Labbe and Kristich 2017). In good agreement, ReoM phosphorylation was also reduced in a *prkA*ΔC mutant (Figure 6D). These findings suggested that lipid II/muropeptides activate PASTA kinases by facilitating their dimerisation. However, when lipid II binding residues in the PASTA domains of *M. tuberculosis* PknB were mutated, the protein became hyperactive instead of inactive, rather suggesting inhibition than activation of the kinase by lipid II (Kaur et al. 2019). In contrast to this, lipid II activated *S. aureus* PknB in vitro, but the degree of activation was only slight (Hardt et al. 2017). Moreover, a structural rather than a regulatory role has recently been proposed for the PASTA domains in *S. pneumoniae* StkP. Through its distal PASTA domain, StkP interacts with the PG hydrolase LytB and positioning of LytB at a defined distance from the membrane, which is determined by the number of PASTA domains, controls cell wall thickness. Obviously, PASTA domains also serve as molecular rulers (Zucchini et al. 2018; Martinez-Caballero et al. 2023) and PASTA kinase activation models in different bacterial species have not reached convergence.

Our results support the idea that *L. monocytogenes* PrkA is constitutively active. Under most conditions and genetic constellations tested, we observed almost complete ReoM phosphorylation. ReoM is a dimer (Hall et al. 2017; Wamp et al. 2020), and therefore existed as ReoM/P~ReoM hetero- or P~ReoM/P~ReoM homodimer, which were the only two ReoM species detected when PrkA was active. Formation of P~ReoM/P~ReoM was reduced during the stationary phase and ReoM/P~ReoM as well as unphosphorylated ReoM accumulated instead. This kinetic was altered upon PrpC depletion suggesting that PrpC also provides a regulatory input and is involved in the shutdown of PG biosynthesis during the transition into stationary phase.

3.3 | MurA Levels Provide a Negative Feed Back on ReoM Phosphorylation

A key result of our study was the observation that ReoM phosphorylation is suppressed in mutants that cannot degrade MurA, that is, in Δ*clpC*, Δ*murZ* or Δ*reoY* mutants. Accumulation of

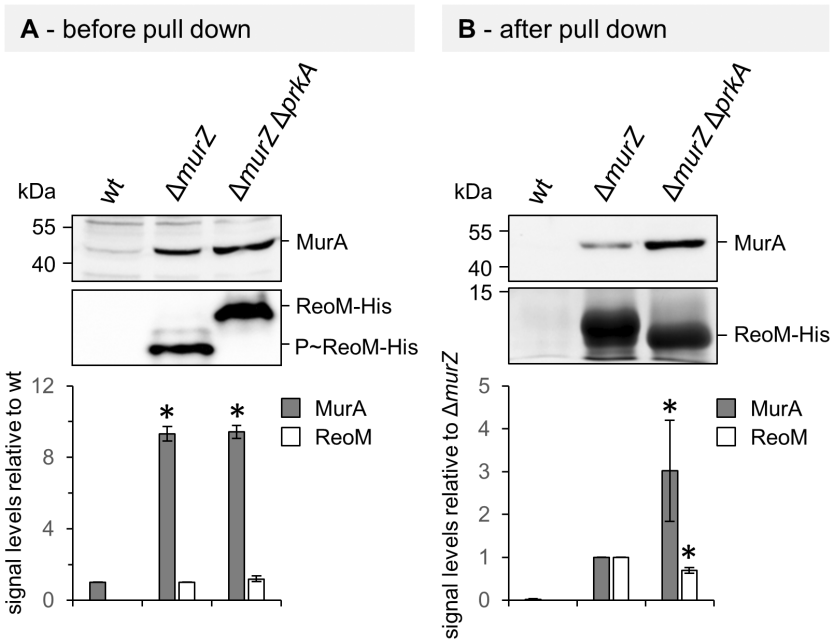

FIGURE 8 | Effect of ReoM phosphorylation on the interaction of ReoM with MurA. Pull down experiment after *in vivo* formaldehyde crosslinking using the *L. monocytogenes* strains EGD-e (wt, control), LMPR25 (Δ*murZ reoM-his*) and LMPR29 (Δ*murZ* Δ*prkA reoM-his*). (A) MurA levels (upper panel) and ReoM phosphorylation (middle panel) prior to crosslinking as determined by Western blotting. For ReoM, samples were separated by native PAGE to allow the separation of ReoM species. Signal intensities were quantified by densitometry and expressed as values relative to wild type (lower panel). Average values and standard deviations are shown. Statistically significant differences are labelled by asterisks ($p < 0.01$, *t*-test with Bonferroni-Holm correction, $n = 3$). (B) Western blot showing MurA levels (upper panel) and SDS-PAGE showing ReoM levels (middle panel) after pull down. MurA and ReoM amounts were quantified (lower panel) as described above but expressed relative to the Δ*murZ* sample. Asterisks indicate significance levels ($p < 0.05$ for MurA, $p < 0.01$ for ReoM, *t*-test, $n = 3$). Please note that the uppermost immunoblots detecting MurA levels before and after pull down in panels A and B were taken from the same gel.

MurA in these mutants was the sole reason for this effect, as *murA* overexpression was sufficient to prevent ReoM phosphorylation. Although overexpression of MurA represents an artificial situation, these results imply that there is a negative feedback mechanism linking the level of MurA to ReoM phosphorylation. Inhibition of PrkA by accumulating lipid II would be a fascinating possibility to explain these observations. In such a scenario, spare MurA molecules generating excess lipid II would be proteolytically degraded due to lipid II-inhibited PrkA that leaves ReoM unphosphorylated. However, our results speak against the existence of such a lipid II-dependent negative feedback loop for three reasons: First, ReoM phosphorylation is still prevented by MurA overexpression in a *prkA*ΔC mutant lacking the PASTA domains. Thus, lipid II binding to PASTA domains cannot be involved. Second, depletion of MurJ activity from Δ*clpC* cells, in which ReoM phosphorylation is prevented due to high MurA levels, does not restore normal ReoM phosphorylation, whereas depletion of MurA from Δ*clpC* cells does. This shows that the signal triggered by excess MurA is generated in the cytoplasmic part of PG biosynthesis somewhere between MurA and MurJ. Third, ReoM phosphorylation depends on the ability of MurA to interact with ReoM. This suggests that MurA itself, its amount or conformation, is possibly sensed by ReoM. MurA also must be able to bind its substrates to prevent ReoM phosphorylation. This is in good agreement with the results reported by Mascari and coworkers, who showed that substrate binding promotes the interaction of *E. faecalis* MurAA with unphosphorylated IreB *in vitro*, whereas phosphorylated IreB could not bind MurA (Mascari, Little, and Kristich 2023). Our *in vivo* results are consistent with this concept, as copurification of MurA with ReoM was sensitive to ReoM phosphorylation. Most of our findings would be compatible with a ReoM partner switching model. Considering the observations that unphosphorylated ReoM forms complexes with PrkA (Wamp et al. 2020) and MurA (Wamp et al. 2022; Mascari, Little, and Kristich 2023), it seems conceivable that PrkA and MurA compete for ReoM as their shared interaction partner. If the amount of MurA is low, ReoM preferably interacts with PrkA leading to ReoM phosphorylation. When the MurA level rises, complex formation of ReoM with MurA becomes more likely and this would initiate MurA degradation. In this sense, the PrkA/ReoM/MurA system would function as a security valve that ensures adaptation of the MurA level to the amount of ReoM. In addition, the ReoM phosphorylation equilibrium responds to alterations in PrpC activity. This observation is particularly evident during the stationary phase, which might reflect a growth phase-specific role of PrpC in the regulation of PG biosynthesis and also would be in good agreement with a strong stationary phase phenotype of a *B. subtilis prpC* mutant (Gaidenko, Kim, and Price 2002). Whether the activity and/or the amount of PrpC is indeed subject to control (Figure 1), is currently not clear, but our data suggest that this possibility should be taken into account. Furthermore, the saturation of MurA with its substrates is integrated into the control network (Figure 7B) (Mascari, Little, and Kristich 2023), but the significance of this is not yet clear.

The partner switching model predicts that ReoM phosphorylation is enhanced in a *murA N197D* mutant because MurA N197D has lower ReoM binding affinity (Wamp et al. 2022). However, we did not observe this (Figure 3A), suggesting that the N197D mutation has a more complex effect on the ReoM phosphorylation equilibrium than previously thought or that the partner switching model needs to be extended. The in vitro reconstitution of this system combined with mathematical modelling of the kinetic parameters could provide an even better understanding of the control of ReoM phosphorylation in the future.

4 | Materials and Methods

4.1 | Bacterial Strains and Growth Conditions

Table 1 lists all bacterial strains and plasmids used in this study. *L. monocytogenes* strains were generally grown in BHI broth or on BHI agar plates at 37°C. Erythromycin (5 μg mL^{-1}), kanamycin (50 μg mL^{-1}), X-Gal (100 μg ml^{-1}) or IPTG (1 mM) were added as indicated. *Escherichia coli* TOP10 was used as the standard cloning host (Sambrook, Fritsch, and Maniatis 1989).

4.2 | General Methods, Manipulation of DNA and Oligonucleotide Primers

Standard methods were used for transformation of *E. coli* and for isolation of plasmid DNA (Sambrook, Fritsch, and Maniatis 1989). Transformation of *L. monocytogenes* was performed using electroporation as described by others (Monk, Gahan, and Hill 2008). PCR, restriction and ligation of DNA were performed following the manufacturer's instructions. All primer sequences are listed in Table 2. Ceftriaxone minimal inhibitory concentrations were determined as described previously using E-test strips with a concentration range of 0.016–256 μg/mL (Bestbiondx, Germany) (Rismondo et al. 2015). Resistance against lysozyme was determined in an autolysis assay as described previously (Rismondo et al. 2018). Minimal inhibitory concentrations of lysozyme were determined as described (Rismondo, Halbedel, and Gründling 2019).

4.3 | Microscopy

Cell membranes were stained by the addition of 1 μL nile red solution (100 μg/mL in DMSO) to 100 μL of exponentially growing bacteria. Images were taken with a Nikon Eclipse Ti microscope coupled to a Nikon DS-MBWc CCD camera and processed using the NIS elements AR software package (Nikon). Cell lengths were measured using the distance measuring tools of NIS elements AR.

4.4 | Construction of Plasmids and Strains

Plasmid pSW51 was constructed for overexpression of ReoM-Strep in *E. coli*. To this end, *reoM* was amplified from chromosomal DNA using SW128/SW129 as the primers. The resulting DNA fragment was cut using SpeI/XhoI and then ligated with the backbone of plasmid pET11a, which had been linearised in a PCR using the oligonucleotides SHW401/SHW402 (introducing the recognition sites for SpeI/XhoI) and cut with the same enzymes.

Plasmid pJR24 was obtained by introducing the T7A mutation into the *reoM* gene of plasmid pJD16 by quikchange mutagenesis and oligonucleotides SW77/SW78 as the primers.

For deletion of *sepF*, plasmid pLR9 was constructed. Up- and downstream fragments of *sepF* were amplified in a PCR using LR13/LR15 and LR16/LR14, respectively, as the primers. Both fragments were fused together by SOE-PCR and the resulting fragment was inserted into pMAD by restriction-free cloning.

Plasmid pLR10, constructed for the deletion of *zapA*, was obtained in a similar way. Here, up- and downstream fragments of *zapA* were amplified in a PCR using the oligonucleotides LR17/LR19 and LR18/LR20, respectively. The two fragments were fused together by SOE-PCR and then inserted into pMAD by restriction-free cloning.

Plasmid pPR30 was constructed for expression of an enzymatically inactive *murA* variant. For this purpose, the C117A mutation was introduced into the *murA* gene present on plasmid pJR82 by quikchange mutagenesis with PR90 and PR91 as the mutagenic primers. Likewise, the K22V and N23A mutations were introduced into *murA* of pJR82 using primers PR122/PR123 (yielding pPR42) and PR118/PR119 (for pPR40), respectively.

Plasmid pPR31 was constructed for deletion of *clpC* from the 10403S chromosome. To this end, regions up- and downstream of *clpC* (*lmrg_02674*) were amplified from 10403S chromosomal DNA using the primer pairs PR86/PR87 and PR88/89 and spliced together in an SOE-PCR. The resulting fragment was then cloned into pMAD using BamHI/NcoI.

For IPTG-dependent expression of *murJ2*, the *murJ2* open reading frame was amplified from 10403S chromosomal DNA using the primer pair ANG3109/ANG3110, the resulting PCR fragment was cut with NcoI and SalI and ligated with pIMK3 that had been cut with the same enzymes.

For the markerless in-frame deletion of *murJ1* and *murJ2*, 1-kb DNA-fragments upstream of *murJ2* and downstream of *murJ1* were amplified by PCR using primer pairs ANG3038/ANG3052 and ANG3053/ANG3048, respectively. The resulting PCR products were fused in a second PCR using primers ANG3038/ANG3048, cut with BamHI and KpnI and ligated with plasmid pKSV7 that had been cut with the same enzymes.

pIMK3 derivatives were brought into *L. monocytogenes* strains by electroporation and transformants were selected on BHI agar plates containing kanamycin at 37°C. Plasmid integration at the tRNA^{Arg} *attB* site was confirmed by PCR. Likewise, pMAD derivatives were introduced into *L. monocytogenes*, but selection was carried out on BHI agar plates containing X-Gal and erythromycin at 30°C. The plasmid integration-excision protocol described by Arnaud, Chastanet, and Debarbouille (2004) was used for gene deletions in the EGD-e background. Plasmid pKSV7-Δ*murJ2-J1* was brought into *L. monocytogenes* 10403S strains by electroporation.

TABLE 1 | Plasmids and strains used in this study.

Name	Relevant characteristics	Source/Reference
Plasmids		
pET11a	*bla* P_{T7} *lacI*	Novagen
pIMK3	P_{help}-*lacO lacI neo*	Monk, Gahan, and Hill (2008)
pKSV7	*bla cat*	Smith and Youngman (1992)
pMAD	*bla erm bgaB*	Arnaud, Chastanet, and Debarbouille (2004)
pJD16	P_{help}-*reoM-his neo*	Wamp et al. (2022)
pJR67	*bla erm bgaB* Δ*murA*	Rismondo, Bender, and Halbedel (2017)
pJR71	P_{help}-*lacO-murZ lacI neo*	Rismondo, Bender, and Halbedel (2017)
pJR82	P_{help}-*lacO-murA lacI neo*	Rismondo, Bender, and Halbedel (2017)
pSH186	*bla erm bgaB* Δ*divIVA*	Halbedel et al. (2012)
pSH554	*bla erm bgaB prkA*ΔC	Fischer et al. (2022)
pSW52	*bla* P_{T7}-*murA-strep lacI*	Wamp et al. (2022)
pIMK3-*murJ2*	P_{help}-*lacO-murJ2 lacI neo*	This work
pKSV7-Δ*J2-J1*	*bla cat* Δ*murJ2-J1* (*lmrg_01341-lmrg_01342*)	This work
pLR9	*bla erm bgaB* Δ*sepF* (*lmo2030*)	This work
pLR10	*bla erm bgaB* Δ*zapA* (*lmo1229*)	This work
pPR24	P_{help}-*reoM T7A-his neo*	This work
pPR30	P_{help}-*lacO-murA C117A lacI neo*	This work
pPR31	*bla erm bgaB* Δ*clpC* (*lmrg_02674*)	This work
pPR40	P_{help}-*lacO-murA N23A lacI neo*	This work
pPR42	P_{help}-*lacO-murA K22V lacI neo*	This work
pSW51	*bla* P_{T7}-*reoM-strep lacI*	This work
L. monocytogenes strains		
EGD-e	Wild-type strain	Glaser et al. (2001)
10403S	Wild-type strain	Becavin et al. (2014)
LMJR4	Δ*gpsB attB*::P_{help}-*lacO-gpsB R25A lacI neo*	Rismondo et al. (2016)
LMJR18	Δ*pbpB2 attB*::P_{help}-*lacO-pbpB2 lacI neo*	Rismondo et al. (2015)
LMJR19	Δ*gpsB*	Rismondo et al. (2016)
LMJR27	Δ*pbpB1 attB*::P_{help}-*lacO-pbpB1 lacI neo*	Rismondo et al. (2015)
LMJR28	Δ*gpsB* Δ*divIVA*	Rismondo et al. (2016)
LMJR68	Δ*gpsB attB*::P_{help}-*lacO-gpsB L24A lacI neo*	Rismondo et al. (2016)
LMJR104	Δ*murZ*	Rismondo, Bender, and Halbedel (2017)
LMJR116	*attB*::P_{help}-*lacO-murA lacI neo*	Rismondo, Bender, and Halbedel (2017)
LMJR123	Δ*murA attB*::P_{help}-*lacO-murA lacI neo*	Rismondo, Bender, and Halbedel (2017)
LMJR130	Δ*gpsB attB*::P_{help}-*lacO-gpsB Y27A lacI neo*	Rismondo et al. (2016)
LMJR131	Δ*gpsB attB*::P_{help}-*lacO-gpsB V32A lacI neo*	Rismondo et al. (2016)
LMJR132	Δ*gpsB attB*::P_{help}-*lacO-gpsB L36A lacI neo*	Rismondo et al. (2016)
LMJR133	Δ*gpsB attB*::P_{help}-*lacO-gpsB D37A lacI neo*	Rismondo et al. (2016)

(Continues)

TABLE 1 | (Continued)

Name	Relevant characteristics	Source/Reference
LMJR134	Δ*gpsB attB*::P_{help}-*lacO-gpsB I40A lacI neo*	Rismondo et al. (2016)
LMJR135	Δ*gpsB attB*::P_{help}-*lacO-gpsB D33A lacI neo*	Rismondo et al. (2016)
LMJR138	Δ*clpC*	Rismondo, Bender, and Halbedel (2017)
LMJR161	Δ*gpsB attB*::P_{help}-*lacO-gpsB T88A lacI neo*	Cleverley et al. (2016)
LMJR162	Δ*gpsB attB*::P_{help}-*lacO-gpsB T88D lacI neo*	Cleverley et al. (2016)
LMJR163	Δ*gpsB attB*::P_{help}-*lacO-gpsB R96A lacI neo*	Rismondo et al. (2016)
LMJR164	Δ*gpsB attB*::P_{help}-*lacO-gpsB E101A lacI neo*	Rismondo et al. (2016)
LMKK35	Δ*minCD*	Kaval, Rismondo, and Halbedel (2014)
LMKK61	Δ*minJ*	Kaval, Rismondo, and Halbedel (2014)
LMS2	Δ*divIVA*	Halbedel et al. (2012)
LMS57	Δ*pbpA1*	Rismondo et al. (2015)
LMS148	Δ*minC*	Kaval, Rismondo, and Halbedel (2014)
LMS163	Δ*pgdA*	Rismondo et al. (2018)
LMS185	Δ*gpsB attB*::P_{help}-*lacO-gpsB F91A lacI neo*	Cleverley et al. (2016)
LMS186	Δ*gpsB attB*::P_{help}-*lacO-gpsB L94A lacI neo*	Cleverley et al. (2016)
LMS187	Δ*gpsB attB*::P_{help}-*lacO-gpsB F105A lacI neo*	Cleverley et al. (2016)
LMS266	Δ*prkA murA N197D*	Wamp et al. (2022)
LMS271	Δ*reoM murA N197D*	Wamp et al. (2022)
LMS278	*prkA*ΔC	Fischer et al. (2022)
LMSW32	Δ*reoY*	Wamp et al. (2020)
LMSW83	Δ*prpC attB*::P_{help}-*lacO-prpC lacI neo*	Wamp et al. (2020)
LMSW84	Δ*prkA attB*::P_{help}-*lacO-prkA lacI neo*	Wamp et al. (2020)
LMSW135	Δ*gpsB* Δ*prpC*	Wamp et al. (2022)
LMSW136	*attB*::P_{help}-*lacO- murA S262L lacI neo*	Wamp et al. (2022)
LMSW137	*attB*::P_{help}-*lacO-murA N197D lacI neo*	Wamp et al. (2022)
LMSW145	Δ*prkA* Δ*murZ*	Wamp et al. (2022)
LMSW156	*murA N197D*	Wamp et al. (2022)
shg21	Δ*gpsB murA N197D*	Wamp et al. (2022)
ANG5115	10403S *attB*::P_{help}-*lacO-murJ2 lacI neo*	pIMK3-*murJ2* → 10403S
ANG5140	10403S Δ*murJ2-murJ1 attB*::P_{help}-*lacO-murJ2 lacI neo*	pKSV7-Δ*J2-J1* ↔ ANG5115
LMJD22	*attB*::P_{help}-*reoM-his neo*	pJD16 → EGD-e
LMLR8	Δ*sepF*	pLR9 ↔ EGD-e
LMLR9	Δ*zapA*	pLR10 ↔ EGD-e
LMPR5	Δ*prkA murA N197D attB*::P_{help}-*reoM-his neo*	pJD16 → LMSW156
LMPR9	*murA N197D attB*::P_{help}-*reoM-his neo*	pJD16 → LMSW156
LMPR10	Δ*gpsB murA N197D attB*::P_{help}-*reoM-his neo*	pJD16 → *shg21*
LMPR24	Δ*gpsB prkA*ΔC *murA N197D*	pSH554 ↔ *shg21*
LMPR25	Δ*murZ attB*::P_{help}-*reoM-his neo*	pJD16 → LMJR104

(Continues)

TABLE 1 | (Continued)

Name	Relevant characteristics	Source/Reference
LMPR27	*prkA*ΔC Δ*divIVA*	pSH186 ↔ LMS278
LMPR28	*prkA*ΔC *murA N197D*	pSH554 ↔ LMSW156
LMPR29	Δ*prkA* Δ*murZ attB*::P_{help}-*reoM-his neo*	pJD16 → LMSW145
LMPR42	*murA N197D attB*::P_{help}-*reoM T7A-his neo*	pPR24 → LMSW156
LMPR48	*murA N197D* Δ*reoM attB*::P_{help}-*reoM T7A-his neo*	pPR24 → LMS271
LMPR49	*prkA*ΔC *attB*::P_{help}-*lacO-murA lacI neo*	pJR82 → LMS278
LMPR50	*attB*::P_{help}-*lacO-murZ lacI neo*	pJR71 → EGDe
LMPR51	*attB*::P_{help}-*lacO-murA C117A lacI neo*	pPR30 → EGDe
LMPR52	Δ*clpC* Δ*murA attB*::P_{help}-*lacO-murA lacI neo*	pJR67 ↔ LMS315
LMPR54	10403S Δ*clpC* Δ*murJ2-J1 attB*::P_{help}-*lacO-murJ2 lacI neo*	pPR31 ↔ ANG5140
LMPR56	*attB*::P_{help}-*lacO-murA N23A lacI neo*	pPR40 → EGD-e
LMPR57	*attB*::P_{help}-*lacO-murA K22V lacI neo*	pPR42 → EGD-e
LMS315	Δ*clpC attB*::P_{help}-*lacO-murA lacI neo*	pJR82 → LMJR138

Note: The arrow (→) stands for a transformation event, and the double arrow (↔) indicates gene deletions obtained by chromosomal insertion and subsequent excision of pMAD/pKSV7 plasmid derivatives (see experimental procedures for details).

The protocol of Camilli, Tilney, and Portnoy (1993) was used for the construction of the *murJ2-J1* deletion by allelic exchange. All gene deletions were confirmed by PCR.

4.5 | Protein Purification and Antibody Generation

ReoM-Strep was overexpressed in *E. coli* BL21, which was cultivated in LB broth containing ampicillin (100 μg/mL) at 37°C. Expression of ReoM-Strep was induced at an optical density of OD_{600} = 0.5 by the addition of 1 mM IPTG (final concentration). The culture was grown overnight at 18°C before cells were harvested by centrifugation. The cell pellet was washed once with ZAP buffer (10 mM Tris/HCl pH 7.5, 200 mM NaCl) and disrupted in ZAP buffer containing 1 mM PMSF using an EmulsiFlex homogeniser (Avestin, Germany). Cell debris was removed by centrifugation (6000 g, 5 min, 4°C) and the resulting supernatant was ultracentrifuged (60,000 g, 30 min 4°C) to remove any remaining particles. ReoM-Strep was purified using affinity chromatography and Strep-Tactin Sepharose (IBA Lifesciences, Germany) according to the manufacturer's instructions. Eluted fractions containing ReoM-Strep were pooled and the buffer was exchanged against PBS using PD10 desalting columns. Samples were aliquoted and stored at −20°C. MurA-Strep was purified from *E. coli* BL21 carrying plasmid pSW52 as described previously (Wamp et al. 2022). ReoM-Strep was used to immunise a rabbit for the generation of a polyclonal antiserum and the IgG fraction was purified from the serum (Biogenes, Germany).

4.6 | MurA Activity Assay

MurA activity was determined by measuring the amount of phosphate released from PEP. For this purpose, 2.5 μg of MurA were mixed with 10 mM uridine 5′-diphospho-*N*-acetylglucosamine (UDP-GlcNAc, Sigma-Aldrich) in a reaction volume of 50 μL containing 100 mM Tris/HCl pH 8.0 and 150 mM NaCl as the buffer and preincubated at 37°C for 15 min. 5 μL 10 mM PEP (Sigma-Aldrich) was added to start the reaction. After 30 min of incubation at room temperature, 800 μL staining solution was added to the reaction. The staining solution was freshly prepared from 10 mL ammonium molybdate solution (4.2 g in 100 mL 4 M HCl), 30 mL malachite green solution (225 mg malachite green in 500 mL H_2O) and 40 μL Triton X-100. Absorption was measured at λ = 660 nm, corrected for background in the absence of UDP-GlcNAc and used to calculate the amount of phosphate released using a standard curve that was generated using solutions with different phosphate concentrations (0–0.5 mM Na_2HPO_4 in 100 mM Tris/HCl pH 8.0, 150 mM NaCl).

4.7 | Isolation of Cellular Proteins

Thirty millilitres of BHI broth were inoculated with an overnight culture to an OD_{600} = 0.05 and grown to an OD_{600} of ~1.0 unless otherwise stated. Cell cultures were harvested by centrifugation, washed with ZAP buffer (50 mM Tris/HCl pH 7.5, 200 mM NaCl), resuspended in 0.5 mL ZAP buffer also containing 1 mM PMSF and disrupted by sonication. Cellular debris was removed by centrifugation and the supernatant was used as total cellular protein extract.

4.8 | Native Page, SDS-PAGE and Western Blotting

To separate proteins on a native gel, 50 μg protein extract was mixed with 6x native loading dye (50 mM Tris/HCl pH 8.5, 0.1% (w/v) bromophenol blue, 10% (w/v) glycerol) and separated on a non-denaturing 15% polyacrylamide (PA) gel (in

TABLE 2 | Primers used in this study.

Name	Sequence (5′ → 3′)
ANG3038	CGCGGATCCCCGGATTTACCTTATGAGCAC
ANG3048	CGGGGTACCGCAAACAGAAAAGCCGATTAC
ANG3052	ATCCTCCTAGCGACTCATAATTTCTGTTACCTCAATTG
ANG3053	GAAATTATGAGTCGCTAGGAGGATTGTATGAAAAAAAC
ANG3109	CATGCCATGGGGAGTTCAAAATTAATGCGAGGGAC
ANG3110	ACGCGTCGACTTAAATCAAATGAAGTTTTTTACGAATTT
LR13	GATCTATCGATGCATGCCATGGTATAAGACAATTTCACCCGGCC
LR14	CGCGTCGGGCGATATCGGATCCAAGAAATCCGTAAGTTGTGGCGTG
LR15	CTTCATCAGTCGACCATTTGTTACACCTCCATATTATCGTC
LR16	AACAAATGGTCGACTGATGAAGTAGAGGTGTGAGCTAG
LR17	CTAGACAGATCTATCGATGCATGCCATGGGAATAATGCTTGGTTCTTTTGC
LR18	CCTCGCGTCGGGCGATATCGGATCCGATACCGCTAATCTTCGTAAAATC
LR19	CATTTAGTCGACCATTTGCCACGTAAATTCCTCCTC
LR20	GTGGCAAATGGTCGACTAAATGATTTTAAATGCGATTATTTTAATTTTAC
PR86	CAGATCTATCGATGCATGCCATGGAGGATTAAAAGTGTGCTTGAAGCGATT
PR87	TACTTAGTCGACCATTGTTGTTTCCTCCTTATCGTA
PR88	ACAATGGTCGACTAAGTAGAAAGCCTTCCTTAATAAAA
PR89	CTCGCGTCGGGCGATATCGGATCCTTGTAAGCGTGAGTTGCGCTGATACT
PR90	CCTGGTGGAGCTGCAATTGGTTCTAGACCTGTT
PR91	AACCAATTGCAGCTCCACCAGGTAAAGCTACACG
PR118	GGTGCCAAAGCTGCTGTATTACCGGTAAT
PR119	TAATACAGCAGCTTTGGCACCTTCCATTT
PR122	TGGAAGGTGCCGTAAATGCTGTATTACCGG
PR123	ATACAGCATTTACGGCACCTTCCATTTTCA
SHW401	GCGCACTAGTCATATGTATATCTCCTTCTTAAAG
SHW402	CGCGCTCGAGCAAAGCCCGAAAGGAAGCTG
SW77	GTAAAACATTGCTTGATCTTTTGAATCCATGGGTTTCAC
SW78	GATCAAGCAATGTTTTACAACTTCGGCG ATGATTC
SW128	GCGCGCACTAGTATGGATTCAAAAGATCAAACAATGTTTTACAAC
SW129	CGCGCGCTCGAGTTATTTTTCGAACTGCGGGTGGCTCCATTTCTCACCAATTTCGTTATTTTTCAGATAC

375 mM Tris/HCl pH 8.8 buffer) that was overlaid with a 5% PA stacking gel in 125 mM Tris/HCl pH 6.8 as the buffer. Both gels were prepared using a 37.5:1 PA solution. Electrophoresis was performed with running buffer (25 mM Tris/HCl pH 8.8, 129 M glycine) at 100 V for 2.5 h at room temperature. For separation under denaturing conditions, protein extracts were separated using standard SDS-PAGE. Transfer of proteins from both types of gels onto positively charged polyvinylidene fluoride membranes was performed using a semi-dry transfer unit. ReoM and MurA were detected using polyclonal rabbit antisera recognising *L. monocytogenes* ReoM (this work) and *B. subtilis* MurAA (Gerth et al. 2004), respectively, as the primary antibodies. An anti-rabbit immunoglobulin G conjugated to horseradish peroxidase was used as the secondary antibody. Detection of antibody–antigen complexes was performed using the ECL chemiluminescence detection system (Thermo Scientific) in a chemiluminescence imager (ChemiDoc MP Imaging System, BioRad). All Western blots shown in this work were representatives of at least three independent experiments.

4.9 | In Vivo Formaldehyde Cross-Linking and Pull Down

L. monocytogenes strains expressing His-tagged bait proteins were cultivated in 500 mL BHI broth containing 1 mM IPTG at 37°C until an OD_{600} of 1.0 was reached. Cultures were treated with formaldehyde at a final concentration of 1% for 30 min. Cross-linking was quenched by glycine addition (50 mM final concentration) for 5 min. Cells were harvested by centrifugation and resuspended in 2 mL UT buffer (0.1 M HEPES, 0.5 M NaCl, 50 mM imidazole, 8 M urea, 1% Triton X-100, 1 mM PMSF, 1 mM dithiothreitol [DTT]). Cell disruption by sonication was performed for 60 min on ice and cell debris was removed by centrifugation. Cleared protein extracts were incubated with 200 µL of MagneHis solution (Promega, USA) overnight, rotating at room temperature. The MagneHis particles were then washed five times with 2 mL of UT buffer. Protein complexes were eluted by incubation in 500 µL elution buffer (0.1 M Tris–HCl pH 7.5, 0.5 M imidazole, 1% SDS, 10 mM DTT) at room temperature for 30 min. Eluates were concentrated five-fold using centrifugal micro-concentrators. Samples were mixed with SDS-PAGE loading dye, and cross-linking was reversed by heating at 95°C for 1 h. Decrosslinked samples were separated by SDS-PAGE and analysed by Western blotting.

4.10 | Purification of His-Tagged ReoM From *L. monocytogenes*

For purification of His-tagged ReoM from *L. monocytogenes* cells under native conditions, we followed the same protocol as outlined above for the pull-down experiments except that the cross-linking and quenching reactions were skipped.

4.11 | In Gel Digestion for Mass Spectrometry

Protein bands were prepared for mass spectrometry using the protocol of Shevchenko et al. (2006). Resulting peptides were desalted using 200 µL StageTips packed with two Empore SPE Disks C18 (3M Purification, Inc., Lexington, USA) according to Rappsilber, Mann, and Ishihama (2007) and concentrated using a vacuum concentrator. Samples were resuspended in 12 µL 0.1% formic acid.

4.12 | nLC-MS/MS

Peptides were analysed on an EASY-nanoLC 1200 (Thermo Fisher Scientific, Bremen, Germany) coupled online to a Q Exactive HF mass spectrometer (Thermo Fisher Scientific, Bremen, Germany). Five-microlitre sample was injected onto a PepSep column (15 cm length, 75 µm i.d., 1.5 µm C18 beads, PepSep, Marslev, Denmark) using a stepped 60 min gradient of 80% acetonitrile (solvent B) in 0.1% formic acid (solvent A) at 300 nL/min flow rate: 4%–8% B in 5:06 min, 8%–26% B in 41:12 min, 26%–31% B in 6:00 min, 31–39% B in 4:12 min, 39%–95% B in 0:10 min, 95% B for 2:20 min, 95%–0% B in 0:10 min and 0% B for 0:50 min. Column temperature was kept at 50°C using a butterfly heater (Phoenix S&T, Chester, PA, USA). The Q Exactive HF was operated in a data-dependent manner in the m/z range of 300–1650. Full scan spectra were recorded with a resolution of 60,000 using an automatic gain control (AGC) target value of 3×10^6 with a maximum injection time of 100 ms. Up to the 10 most intense 2+–4+ charged ions were selected for higher-energy c-trap dissociation (HCD) with a normalised collision energy (NCE) of 27%. Fragment spectra were recorded at an isolation width of 2 Th and a resolution of 30,000@200 m/z using an AGC target value of 1×10^5 with a maximum injection time of 50 ms. The minimum MS^2 target value was set to 1×10^4. Once fragmented, peaks were dynamically excluded from precursor selection for 30 s within a 10 ppm window. Peptides were ionised using electrospray with a stainless-steel emitter, i.d. 30 µm, (Proxeon, Odense, Denmark) at a spray voltage of 2.1 kV and a heated capillary temperature of 275°C.

4.13 | Analysis of Mass Spectrometric Data

The mass spectra were analysed using Proteome Discoverer 2.5 (Thermo Fisher Scientific, Bremen, Germany). Spectra were analysed using SequestHT with a tolerance of 10 ppm in MS^1 and 0.02 Da in HCD MS^2 mode, strict trypsin specificity and allowing up to two missed cleavage sites. Cysteine carbamidomethylation was set as a fixed modification and oxidation (M), phosphorylation (S,T,Y) as well as N-terminal acetylation and loss of initial methionine as variable modifications. Peptides were identified at 1% false discovery rate using Percolator and quantified using Minora feature detector with default settings. The localisation of phosphorylation sites was scored using ptmRS. Afterwards, phosphorylated peptides were further filtered using the cross-correlation score (Xcorr) ($z=2>2$, $z=3>2.3$, $z=4>2.6$), best site probability (>0.8) and MS^1 mass accuracy (<5 ppm) to retrieve a list of high confident phosphopeptides.

Author Contributions

Patricia Rothe: investigation, validation, formal analysis, visualization, writing – review and editing, writing – original draft, data curation, methodology. **Sabrina Wamp:** investigation, validation, formal analysis, visualization, writing – review and editing, data curation, methodology. **Lisa Rosemeyer:** investigation, validation, formal analysis, writing – review and editing, data curation. **Jeanine Rismondo:** investigation, validation, formal analysis, writing – review and editing, writing – original draft, data curation, methodology. **Joerg Doellinger:** investigation, validation, methodology, formal analysis, writing – original draft, writing – review and editing, data curation. **Angelika Gründling:** supervision, project administration, writing – review and editing. **Sven Halbedel:** conceptualization, data curation, investigation, validation, formal analysis, supervision, funding acquisition, visualization, project administration, writing – review and editing, writing – original draft.

Acknowledgements

This work was funded by DFG grants HA 6830/1-2 and HA 6830/4-1 (to S.H.). The authors would like to thank Janina Döhling for her help with some experiments. Open Access funding enabled and organized by Projekt DEAL.

Data Availability Statement

The data that support the findings of this study are available from the corresponding author upon reasonable request.

References

Arnaud, M., A. Chastanet, and M. Debarbouille. 2004. "New Vector for Efficient Allelic Replacement in Naturally Nontransformable, Low-GC-Content, Gram-Positive Bacteria." *Applied and Environmental Microbiology* 70: 6887–6891. https://doi.org/10.1128/AEM.70.11.6887-6891.2004.

Asai, K. 2018. "Anti-Sigma Factor-Mediated Cell Surface Stress Responses in *Bacillus subtilis*." *Genes & Genetic Systems* 92: 223–234. https://doi.org/10.1266/ggs.17-00046.

Barreteau, H., A. Kovac, A. Boniface, M. Sova, S. Gobec, and D. Blanot. 2008. "Cytoplasmic Steps of Peptidoglycan Biosynthesis." *FEMS Microbiology Reviews* 32: 168–207. https://doi.org/10.1111/j.1574-6976.2008.00104.x.

Barthe, P., G. V. Mukamolova, C. Roumestand, and M. Cohen-Gonsaud. 2010. "The Structure of PknB Extracellular PASTA Domain From Mycobacterium Tuberculosis Suggests a Ligand-Dependent Kinase Activation." *Structure* 18: 606–615. https://doi.org/10.1016/j.str.2010.02.013.

Bartlett, T. M., T. A. Sisley, A. Mychack, et al. 2024. "FacZ Is a GpsB-Interacting Protein That Prevents Aberrant Division-Site Placement in *Staphylococcus aureus*." *Nature Microbiology* 9: 801–813. https://doi.org/10.1038/s41564-024-01607-y.

Becavin, C., C. Bouchier, P. Lechat, et al. 2014. "Comparison of Widely Used *Listeria monocytogenes* Strains EGD, 10403S, and EGD-e Highlights Genomic Variations Underlying Differences in Pathogenicity." *MBio* 5: e00969-00914. https://doi.org/10.1128/mBio.00969-14.

Beilharz, K., L. Novakova, D. Fadda, P. Branny, O. Massidda, and J. W. Veening. 2012. "Control of Cell Division in *Streptococcus pneumoniae* by the Conserved Ser/Thr Protein Kinase StkP." *Proceedings of the National Academy of Sciences of the United States of America* 109: E905–E913. https://doi.org/10.1073/pnas.1119172109.

Blake, K. L., A. J. O'Neill, D. Mengin-Lecreulx, et al. 2009. "The Nature of *Staphylococcus aureus* MurA and MurZ and Approaches for Detection of Peptidoglycan Biosynthesis Inhibitors." *Molecular Microbiology* 72: 335–343. https://doi.org/10.1111/j.1365-2958.2009.06648.x.

Boutte, C. C., C. E. Baer, K. Papavinasasundaram, et al. 2016. "A Cytoplasmic Peptidoglycan Amidase Homologue Controls Mycobacterial Cell Wall Synthesis." *eLife* 5: e14590. https://doi.org/10.7554/eLife.14590.

Brogan, A. P., and D. Z. Rudner. 2023. "Regulation of Peptidoglycan Hydrolases: Localization, Abundance, and Activity." *Current Opinion in Microbiology* 72: 102279. https://doi.org/10.1016/j.mib.2023.102279.

Camilli, A., L. G. Tilney, and D. A. Portnoy. 1993. "Dual Roles of *plcA* in *Listeria monocytogenes* Pathogenesis." *Molecular Microbiology* 8: 143–157. https://doi.org/10.1111/j.1365-2958.1993.tb01211.x.

Claessen, D., R. Emmins, L. W. Hamoen, R. A. Daniel, J. Errington, and D. H. Edwards. 2008. "Control of the Cell Elongation-Division Cycle by Shuttling of PBP1 Protein in *Bacillus subtilis*." *Molecular Microbiology* 68: 1029–1046. https://doi.org/10.1111/j.1365-2958.2008.06210.x.

Cleverley, R. M., J. Rismondo, M. P. Lockhart-Cairns, et al. 2016. "Subunit Arrangement in GpsB, a Regulator of Cell Wall Biosynthesis." *Microbial Drug Resistance* 22: 446–460. https://doi.org/10.1089/mdr.2016.0050.

Cleverley, R. M., Z. J. Rutter, J. Rismondo, et al. 2019. "The Cell Cycle Regulator GpsB Functions as Cytosolic Adaptor for Multiple Cell Wall Enzymes." *Nature Communications* 10: 261. https://doi.org/10.1038/s41467-018-08056-2.

Deng, M. D., A. D. Grund, S. L. Wassink, et al. 2006. "Directed Evolution and Characterization of *Escherichia coli* Glucosamine Synthase." *Biochimie* 88: 419–429. https://doi.org/10.1016/j.biochi.2005.10.002.

Du, W., J. R. Brown, D. R. Sylvester, et al. 2000. "Two Active Forms of UDP-N-Acetylglucosamine Enolpyruvyl Transferase in Gram-Positive Bacteria." *Journal of Bacteriology* 182: 4146–4152. https://doi.org/10.1128/jb.182.15.4146-4152.2000.

Egan, A. J., R. M. Cleverley, K. Peters, R. J. Lewis, and W. Vollmer. 2017. "Regulation of Bacterial Cell Wall Growth." *FEBS Journal* 284: 851–867. https://doi.org/10.1111/febs.13959.

Egan, A. J. F., J. Errington, and W. Vollmer. 2020. "Regulation of Peptidoglycan Synthesis and Remodelling." *Nature Reviews. Microbiology* 18: 446–460. https://doi.org/10.1038/s41579-020-0366-3.

Emami, K., A. Guyet, Y. Kawai, et al. 2017. "RodA as the Missing Glycosyltransferase in *Bacillus subtilis* and Antibiotic Discovery for the Peptidoglycan Polymerase Pathway." *Nature Microbiology* 2: 16253. https://doi.org/10.1038/nmicrobiol.2016.253.

Fischer, M. A., T. Engelgeh, P. Rothe, S. Fuchs, A. Thürmer, and S. Halbedel. 2022. "*Listeria monocytogenes* Genes Supporting Growth Under Standard Laboratory Cultivation Conditions and During Macrophage Infection." *Genome Research* 32: 1711–1726. https://doi.org/10.1101/gr.276747.122.

Fleurie, A., S. Manuse, C. Zhao, et al. 2014. "Interplay of the Serine/Threonine-Kinase StkP and the Paralogs DivIVA and GpsB in Pneumococcal Cell Elongation and Division." *PLoS Genetics* 10: e1004275. https://doi.org/10.1371/journal.pgen.1004275.

Foulquier, E., F. Pompeo, D. Byrne, H. P. Fierobe, and A. Galinier. 2020. "Uridine Diphosphate N-Acetylglucosamine Orchestrates the Interaction of GlmR With Either YvcJ or GlmS in *Bacillus subtilis*." *Scientific Reports* 10: 15938. https://doi.org/10.1038/s41598-020-72854-2.

Gaidenko, T. A., T. J. Kim, and C. W. Price. 2002. "The PrpC Serine-Threonine Phosphatase and PrkC Kinase Have Opposing Physiological Roles in Stationary-Phase *Bacillus subtilis* Cells." *Journal of Bacteriology* 184: 6109–6114. https://doi.org/10.1128/jb.184.22.6109-6114.2002.

Galinier, A., C. Delan-Forino, E. Foulquier, H. Lakhal, and F. Pompeo. 2023. "Recent Advances in Peptidoglycan Synthesis and Regulation in Bacteria." *Biomolecules* 13: 720. https://doi.org/10.3390/biom13050720.

Gautam, A., P. Rishi, and R. Tewari. 2011. "UDP-N-Acetylglucosamine Enolpyruvyl Transferase as a Potential Target for Antibacterial Chemotherapy: Recent Developments." *Applied Microbiology and Biotechnology* 92: 211–225. https://doi.org/10.1007/s00253-011-3512-z.

Gee, C. L., K. G. Papavinasasundaram, S. R. Blair, et al. 2012. "A Phosphorylated Pseudokinase Complex Controls Cell Wall Synthesis in Mycobacteria." *Science Signaling* 5: ra7. https://doi.org/10.1126/scisignal.2002525.

Gerth, U., J. Kirstein, J. Mostertz, et al. 2004. "Fine-Tuning in Regulation of Clp Protein Content in *Bacillus subtilis*." *Journal of Bacteriology* 186: 179–191. https://doi.org/10.1128/jb.186.1.179-191.2004.

Glaser, P., L. Frangeul, C. Buchrieser, et al. 2001. "Comparative Genomics of *Listeria* Species." *Science* 294: 849–852. https://doi.org/10.1126/science.1063447294/5543/849.

Graham, J. W., M. G. Lei, and C. Y. Lee. 2013. "Trapping and Identification of Cellular Substrates of the *Staphylococcus aureus* ClpC Chaperone." *Journal of Bacteriology* 195: 4506–4516. https://doi.org/10.1128/JB.00758-13.

Halbedel, S., B. Hahn, R. A. Daniel, and A. Flieger. 2012. "DivIVA Affects Secretion of Virulence-Related Autolysins in *Listeria monocytogenes*." *Molecular Microbiology* 83: 821–839. https://doi.org/10.1111/j.1365-2958.2012.07969.x.

Halbedel, S., and R. J. Lewis. 2019. "Structural Basis for Interaction of DivIVA/GpsB Proteins With Their Ligands." *Molecular Microbiology* 111: 1404–1415. https://doi.org/10.1111/mmi.14244.

Hall, C. L., B. L. Lytle, D. Jensen, et al. 2017. "Structure and Dimerization of IreB, a Negative Regulator of Cephalosporin Resistance in *Enterococcus faecalis*." *Journal of Molecular Biology* 429: 2324–2336. https://doi.org/10.1016/j.jmb.2017.05.019.

Hall, C. L., M. Tschannen, E. A. Worthey, and C. J. Kristich. 2013. "IreB, a ser/Thr Kinase Substrate, Influences Antimicrobial Resistance in *Enterococcus faecalis*." *Antimicrobial Agents and Chemotherapy* 57: 6179–6186. https://doi.org/10.1128/AAC.01472-13.

Hardt, P., I. Engels, M. Rausch, et al. 2017. "The Cell Wall Precursor Lipid II Acts as a Molecular Signal for the Ser/Thr Kinase PknB of *Staphylococcus aureus*." *International Journal of Medical Microbiology* 307: 1–10. https://doi.org/10.1016/j.ijmm.2016.12.001.

Helmann, J. D. 2016. "*Bacillus Subtilis* Extracytoplasmic Function (ECF) Sigma Factors and Defense of the Cell Envelope." *Current Opinion in Microbiology* 30: 122–132. https://doi.org/10.1016/j.mib.2016.02.002.

Hottmann, I., M. Borisova, C. Schaffer, and C. Mayer. 2021. "Peptidoglycan Salvage Enables the Periodontal Pathogen *Tannerella forsythia* to Survive Within the Oral Microbial Community." *Microbial Physiology* 31: 123–134. https://doi.org/10.1159/000516751.

Kaur, P., M. Rausch, B. Malakar, et al. 2019. "LipidII Interaction With Specific Residues of *Mycobacterium tuberculosis* PknB Extracytoplasmic Domain Governs Its Optimal Activation." *Nature Communications* 10: 1231. https://doi.org/10.1038/s41467-019-09223-9.

Kaval, K. G., J. Rismondo, and S. Halbedel. 2014. "A Function of DivIVA in *Listeria monocytogenes* Division Site Selection." *Molecular Microbiology* 94: 637–654. https://doi.org/10.1111/mmi.12784.

Kelliher, J. L., M. E. Daanen, and J.-D. Sauer. 2023. "GpsB Control of PASTA Kinase Activity in *Listeria monocytogenes* Influences Peptidoglycan Synthesis During Cell Wall Stress and Cytosolic Survival." *bioRxiv* 2023.2006.2012.544644. https://doi.org/10.1101/2023.06.12.544644.

Kelliher, J. L., C. M. Grunenwald, R. R. Abrahams, et al. 2021. "PASTA Kinase-Dependent Control of Peptidoglycan Synthesis via ReoM Is Required for Cell Wall Stress Responses, Cytosolic Survival, and Virulence in *Listeria monocytogenes*." *PLoS Pathogens* 17: e1009881. https://doi.org/10.1371/journal.ppat.1009881.

Kieser, K. J., C. C. Boutte, J. C. Kester, et al. 2015. "Phosphorylation of the Peptidoglycan Synthase PonA1 Governs the Rate of Polar Elongation in Mycobacteria." *PLoS Pathogens* 11: e1005010. https://doi.org/10.1371/journal.ppat.1005010.

Kim, D. H., W. J. Lees, K. E. Kempsell, W. S. Lane, K. Duncan, and C. T. Walsh. 1996. "Characterization of a Cys115 to asp Substitution in the *Escherichia coli* Cell Wall Biosynthetic Enzyme UDP-GlcNAc Enolpyruvyl Transferase (MurA) That Confers Resistance to Inactivation by the Antibiotic Fosfomycin." *Biochemistry* 35: 4923–4928. https://doi.org/10.1021/bi952937w.

Kock, H., U. Gerth, and M. Hecker. 2004. "MurAA, Catalysing the First Committed Step in Peptidoglycan Biosynthesis, Is a Target of Clp-Dependent Proteolysis in *Bacillus subtilis*." *Molecular Microbiology* 51: 1087–1102.

Labbe, B. D., and C. J. Kristich. 2017. "Growth- and Stress-Induced PASTA Kinase Phosphorylation in *Enterococcus faecalis*." *Journal of Bacteriology* 199: e00363-17. https://doi.org/10.1128/JB.00363-17.

Martinez-Caballero, S., C. Freton, R. Molina, et al. 2023. "Molecular Basis of the Final Step of Cell Division in *Streptococcus pneumoniae*." *Cell Reports* 42: 112756. https://doi.org/10.1016/j.celrep.2023.112756.

Mascari, C. A., J. L. Little, and C. J. Kristich. 2023. "PASTA-Kinase-Mediated Signaling Drives Accumulation of the Peptidoglycan Synthesis Protein MurAA to Promote Cephalosporin Resistance in *Enterococcus faecalis*." *Molecular Microbiology* 120: 811–829. https://doi.org/10.1111/mmi.15150.

Meeske, A. J., E. P. Riley, W. P. Robins, et al. 2016. "SEDS Proteins Are a Widespread Family of Bacterial Cell Wall Polymerases." *Nature* 537: 634–638. https://doi.org/10.1038/nature19331.

Meeske, A. J., L. T. Sham, H. Kimsey, et al. 2015. "MurJ and a Novel Lipid II Flippase Are Required for Cell Wall Biogenesis in *Bacillus subtilis*." *Proceedings of the National Academy of Sciences of the United States of America* 112: 6437–6442. https://doi.org/10.1073/pnas.1504967112.

Minton, N. E., D. Djoric, J. Little, and C. J. Kristich. 2022. "GpsB Promotes PASTA Kinase Signaling and Cephalosporin Resistance in *Enterococcus faecalis*." *Journal of Bacteriology* 204: e0030422. https://doi.org/10.1128/jb.00304-22.

Mir, M., J. Asong, X. Li, J. Cardot, G. J. Boons, and R. N. Husson. 2011. "The Extracytoplasmic Domain of the *Mycobacterium tuberculosis* Ser/Thr Kinase PknB Binds Specific Muropeptides and Is Required for PknB Localization." *PLoS Pathogens* 7: e1002182. https://doi.org/10.1371/journal.ppat.1002182.

Mizyed, S., A. Oddone, B. Byczynski, D. W. Hughes, and P. J. Berti. 2005. "UDP-N-Acetylmuramic Acid (UDP-MurNAc) Is a Potent Inhibitor of MurA (Enolpyruvyl-UDP-GlcNAc Synthase)." *Biochemistry* 44: 4011–4017. https://doi.org/10.1021/bi047704w.

Monk, I. R., C. G. Gahan, and C. Hill. 2008. "Tools for Functional Postgenomic Analysis of *Listeria monocytogenes*." *Applied and Environmental Microbiology* 74: 3921–3934. https://doi.org/10.1128/AEM.00314-08.

Pallova, P., K. Hercik, L. Saskova, L. Novakova, and P. Branny. 2007. "A Eukaryotic-Type Serine/Threonine Protein Kinase StkP of *Streptococcus pneumoniae* Acts as a Dimer in Vivo." *Biochemical and Biophysical Research Communications* 355: 526–530. https://doi.org/10.1016/j.bbrc.2007.01.184.

Pompeo, F., D. Byrne, D. Mengin-Lecreulx, and A. Galinier. 2018. "Dual Regulation of Activity and Intracellular Localization of the PASTA Kinase PrkC During *Bacillus subtilis* Growth." *Scientific Reports* 8: 1660. https://doi.org/10.1038/s41598-018-20145-2.

Pompeo, F., E. Foulquier, B. Serrano, C. Grangeasse, and A. Galinier. 2015. "Phosphorylation of the Cell Division Protein GpsB Regulates PrkC Kinase Activity Through a Negative Feedback Loop in *Bacillus subtilis*." *Molecular Microbiology* 97: 139–150. https://doi.org/10.1111/mmi.13015.

Rakette, S., S. Donat, K. Ohlsen, and T. Stehle. 2012. "Structural Analysis of *Staphylococcus aureus* Serine/Threonine Kinase PknB." *PLoS ONE* 7: e39136. https://doi.org/10.1371/journal.pone.0039136.

Rappsilber, J., M. Mann, and Y. Ishihama. 2007. "Protocol for Micro-Purification, Enrichment, pre-Fractionation and Storage of Peptides for Proteomics Using StageTips." *Nature Protocols* 2: 1896–1906. https://doi.org/10.1038/nprot.2007.261.

Rismondo, J., J. K. Bender, and S. Halbedel. 2017. "Suppressor Mutations Linking *gpsB* With the First Committed Step of Peptidoglycan Biosynthesis in *Listeria monocytogenes*." *Journal of Bacteriology* 199: e00393-16. https://doi.org/10.1128/JB.00393-16.

Rismondo, J., R. M. Cleverley, H. V. Lane, et al. 2016. "Structure of the Bacterial Cell Division Determinant GpsB and Its Interaction With Penicillin-Binding Proteins." *Molecular Microbiology* 99: 978–998. https://doi.org/10.1111/mmi.13279.

Rismondo, J., S. Halbedel, and A. Gründling. 2019. "Cell Shape and Antibiotic Resistance Are Maintained by the Activity of Multiple FtsW and RodA Enzymes in *Listeria monocytogenes*." *MBio* 10: e01448-19. https://doi.org/10.1128/mBio.01448-19.

Rismondo, J., L. Moller, C. Aldridge, J. Gray, W. Vollmer, and S. Halbedel. 2015. "Discrete and Overlapping Functions of Peptidoglycan Synthases in Growth, Cell Division and Virulence of *Listeria monocytogenes*." *Molecular Microbiology* 95: 332–351. https://doi.org/10.1111/mmi.12873.

Rismondo, J., S. Wamp, C. Aldridge, W. Vollmer, and S. Halbedel. 2018. "Stimulation of PgdA-Dependent Peptidoglycan N-Deacetylation by GpsB-PBP A1 in *Listeria monocytogenes*." *Molecular Microbiology* 107: 472–487. https://doi.org/10.1111/mmi.13893.

Ruiz, N. 2015. "Lipid Flippases for Bacterial Peptidoglycan Biosynthesis." *Lipid Insights* 8: 21–31. https://doi.org/10.4137/LPI.S31783.

Sacco, M. D., L. R. Hammond, R. E. Noor, et al. 2024. "*Staphylococcus aureus* FtsZ and PBP4 Bind to the Conformationally Dynamic N-Terminal Domain of GpsB." *eLife* 13: e85579. https://doi.org/10.7554/eLife.85579.

Sambrook, J., E. F. Fritsch, and T. Maniatis. 1989. *Molecular Cloning: A Laboratory Manual*, 3. Cold Spring Harbor, NY: Cold Spring Harbor Laboratory Press.

Samland, A. K., N. Amrhein, and P. Macheroux. 1999. "Lysine 22 in UDP-N-Acetylglucosamine Enolpyruvyl Transferase From *Enterobacter cloacae* Is Crucial for Enzymatic Activity and the Formation of Covalent Adducts With the Substrate Phosphoenolpyruvate and the Antibiotic Fosfomycin." *Biochemistry* 38: 13162–13169. https://doi.org/10.1021/bi991041e.

Samland, A. K., T. Etezady-Esfarjani, N. Amrhein, and P. Macheroux. 2001. "Asparagine 23 and Aspartate 305 Are Essential Residues in the Active Site of UDP-N-Acetylglucosamine Enolpyruvyl Transferase From *Enterobacter cloacae*." *Biochemistry* 40: 1550–1559. https://doi.org/10.1021/bi001490a.

Sauvage, E., F. Kerff, M. Terrak, J. A. Ayala, and P. Charlier. 2008. "The Penicillin-Binding Proteins: Structure and Role in Peptidoglycan Biosynthesis." *FEMS Microbiology Reviews* 32: 234–258. https://doi.org/10.1111/j.1574-6976.2008.00105.x.

Schönbrunn, E., S. Eschenburg, F. Krekel, K. Luger, and N. Amrhein. 2000. "Role of the Loop Containing Residue 115 in the Induced-Fit Mechanism of the Bacterial Cell Wall Biosynthetic Enzyme MurA." *Biochemistry* 39: 2164–2173. https://doi.org/10.1021/bi991091j.

Schönbrunn, E., D. I. Svergun, N. Amrhein, and M. H. Koch. 1998. "Studies on the Conformational Changes in the Bacterial Cell Wall Biosynthetic Enzyme UDP-N-Acetylglucosamine Enolpyruvyltransferase (MurA)." *European Journal of Biochemistry* 253: 406–412. https://doi.org/10.1046/j.1432-1327.1998.2530406.x.

Shevchenko, A., H. Tomas, J. Havlis, J. V. Olsen, and M. Mann. 2006. "In-Gel Digestion for Mass Spectrometric Characterization of Proteins and Proteomes." *Nature Protocols* 1: 2856–2860. https://doi.org/10.1038/nprot.2006.468.

Skarzynski, T., D. H. Kim, W. J. Lees, C. T. Walsh, and K. Duncan. 1998. "Stereochemical Course of Enzymatic Enolpyruvyl Transfer and Catalytic Conformation of the Active Site Revealed by the Crystal Structure of the Fluorinated Analogue of the Reaction Tetrahedral Intermediate Bound to the Active Site of the C115A Mutant of MurA." *Biochemistry* 37: 2572–2577. https://doi.org/10.1021/bi9722608.

Skarzynski, T., A. Mistry, A. Wonacott, S. E. Hutchinson, V. A. Kelly, and K. Duncan. 1996. "Structure of UDP-*N*-Acetylglucosamine Enolpyruvyl Transferase, an Enzyme Essential for the Synthesis of Bacterial Peptidoglycan, Complexed With Substrate UDP-N-Acetylglucosamine and the Drug Fosfomycin." *Structure* 4: 1465–1474.

Smith, K., and P. Youngman. 1992. "Use of a New Integrational Vector to Investigate Compartment-Specific Expression of the *Bacillus subtilis* spoIIM Gene." *Biochimie* 74: 705–711. https://doi.org/10.1016/0300-9084(92)90143-3.

Sun, Y., S. Hurlimann, and E. Garner. 2023. "Growth Rate Is Modulated by Monitoring Cell Wall Precursors in *Bacillus subtilis*." *Nature Microbiology* 8: 469–480. https://doi.org/10.1038/s41564-023-01329-7.

Taguchi, A., M. A. Welsh, L. S. Marmont, et al. 2019. "FtsW Is a Peptidoglycan Polymerase That Is Functional Only in Complex With Its Cognate Penicillin-Binding Protein." *Nature Microbiology* 4: 587–594. https://doi.org/10.1038/s41564-018-0345-x.

Takada, H., and H. Yoshikawa. 2018. "Essentiality and Function of WalK/WalR Two-Component System: The Past, Present, and Future of Research." *Bioscience, Biotechnology, and Biochemistry* 82: 741–751. https://doi.org/10.1080/09168451.2018.1444466.

Teo, A. C., and D. I. Roper. 2015. "Core Steps of Membrane-Bound Peptidoglycan Biosynthesis: Recent Advances, Insight and Opportunities." *Antibiotics (Basel)* 4: 495–520. https://doi.org/10.3390/antibiotics4040495.

Timmler, S. B., S. L. Kellogg, S. N. Atkinson, J. L. Little, D. Djoric, and C. J. Kristich. 2022. "CroR Regulates Expression of *pbp4(5)* to Promote Cephalosporin Resistance in *Enterococcus faecalis*." *MBio* 13: e0111922. https://doi.org/10.1128/mbio.01119-22.

Tsui, H. T., M. Joseph, J. J. Zheng, et al. 2023. "Negative Regulation of MurZ and MurA Underlies the Essentiality of GpsB- and StkP-Mediated Protein Phosphorylation in *Streptococcus pneumoniae* D39." *Molecular Microbiology* 120: 351–383. https://doi.org/10.1111/mmi.15122.

van Baarle, S., I. N. Celik, K. G. Kaval, M. Bramkamp, L. W. Hamoen, and S. Halbedel. 2013. "Protein-Protein Interaction Domains of *Bacillus subtilis* DivIVA." *Journal of Bacteriology* 195: 1012–1021. https://doi.org/10.1128/JB.02171-12.

VanZeeland, N. E., K. M. Schultz, C. S. Klug, and C. J. Kristich. 2023. "Multisite Phosphorylation Regulates GpsB Function in Cephalosporin Resistance of *Enterococcus faecalis*." *Journal of Molecular Biology* 435: 168216. https://doi.org/10.1016/j.jmb.2023.168216.

Vesic, D., and C. J. Kristich. 2012. "MurAA Is Required for Intrinsic Cephalosporin Resistance of *Enterococcus faecalis*." *Antimicrobial Agents and Chemotherapy* 56: 2443–2451. https://doi.org/10.1128/AAC.05984-11.

Wamp, S., P. Rothe, D. Stern, G. Holland, J. Döhling, and S. Halbedel. 2022. "MurA Escape Mutations Uncouple Peptidoglycan Biosynthesis From PrkA Signaling." *PLoS Pathogens* 18: e1010406. https://doi.org/10.1371/journal.ppat.1010406.

Wamp, S., Z. J. Rutter, J. Rismondo, et al. 2020. "PrkA Controls Peptidoglycan Biosynthesis Through the Essential Phosphorylation of ReoM." *eLife* 9: e56048. https://doi.org/10.7554/eLife.56048.

Wanke, C., and N. Amrhein. 1993. "Evidence That the Reaction of the UDP-N-Acetylglucosamine 1-Carboxyvinyltransferase Proceeds Through the O-Phosphothioketal of Pyruvic Acid Bound to Cys115 of the Enzyme." *European Journal of Biochemistry* 218: 861–870. https://doi.org/10.1111/j.1432-1033.1993.tb18442.x.

Winkler, W. C., A. Nahvi, A. Roth, J. A. Collins, and R. R. Breaker. 2004. "Control of Gene Expression by a Natural Metabolite-Responsive Ribozyme." *Nature* 428: 281–286. https://doi.org/10.1038/nature02362.

Zhu, J. Y., Y. Yang, H. Han, et al. 2012. "Functional Consequence of Covalent Reaction of Phosphoenolpyruvate With UDP-N-Acetylglucosamine 1-Carboxyvinyltransferase (MurA)." *Journal of Biological Chemistry* 287: 12657–12667. https://doi.org/10.1074/jbc.M112.342725.

Zucchini, L., C. Mercy, P. S. Garcia, et al. 2018. "PASTA Repeats of the Protein Kinase StkP Interconnect Cell Constriction and Separation of *Streptococcus pneumoniae*." *Nature Microbiology* 3: 197–209. https://doi.org/10.1038/s41564-017-0069-3.

Supporting Information

Additional supporting information can be found online in the Supporting Information section.